



Article

Gene-Specific Discriminative Echocardiogram Findings in Hypertrophic Cardiomyopathy Determined Using Artificial Intelligence: A Pilot Study

Mila Glavaški ^{1,*} , Aleksandra Ilić ^{1,2} and Lazar Velicki ^{1,2} ¹ Faculty of Medicine, University of Novi Sad, Hajduk Veljkova 3, 21000 Novi Sad, Serbia² Institute of Cardiovascular Diseases Vojvodina, Put Doktora Goldmana 4, 21204 Sremska Kamenica, Serbia

* Correspondence: milaglavaski@yahoo.com

Abstract: Hypertrophic cardiomyopathy (HCM) is among the most common forms of cardiomyopathies, with a prevalence of 1:200 to 1:500 people. HCM is caused by variants in genes encoding cardiac sarcomeric proteins, of which a majority reside in *MYH7*, *MYBPC3*, and *TNNT2*. Up to 40% of the HCM cases do not have any known HCM variant. Genotype–phenotype associations in HCM remain incompletely understood. This study involved two visits of 46 adult patients with a confirmed diagnosis of HCM. In total, 174 genes were analyzed on the Next-Generation Sequencing platform, and transthoracic echocardiography was performed. Gene-specific discriminative echocardiogram findings were identified using the computer vision library Fast AI. This was accomplished with the generation of deep learning models for the classification of ultrasonic images based on the underlying genotype and a later analysis of the most decisive image regions. Gene-specific echocardiogram findings were identified: for variants in the *MYH7* gene (vs. variant not detected), the most discriminative structures were the septum, left ventricular outflow tract (LVOT) segment, anterior wall, apex, right ventricle, and mitral apparatus; for variants in *MYBPC3* gene (vs. variant not detected) these were the septum, left ventricle, and left ventricle/chamber; while for variants in the *TNNT2* gene (vs. variant not detected), the most discriminative structures were the septum and right ventricle.



Citation: Glavaški, M.; Ilić, A.; Velicki, L. Gene-Specific Discriminative Echocardiogram Findings in Hypertrophic Cardiomyopathy Determined Using Artificial Intelligence: A Pilot Study. *Cardiogenetics* **2024**, *14*, 1–25. <https://doi.org/10.3390/cardiogenetics14010001>

Academic Editor: Giuseppe Limongelli

Received: 23 April 2023

Revised: 19 December 2023

Accepted: 20 December 2023

Published: 25 December 2023



Copyright: © 2023 by the authors. Licensee MDPI, Basel, Switzerland. This article is an open access article distributed under the terms and conditions of the Creative Commons Attribution (CC BY) license (<https://creativecommons.org/licenses/by/4.0/>).

Keywords: hypertrophic cardiomyopathy; gene; *MYH7*; *MYBPC3*; *TNNT2*; variant; echocardiogram; echocardiography; artificial intelligence; computer vision

1. Introduction

Hypertrophic cardiomyopathy (HCM) is among the most common forms of cardiomyopathy [1,2], with a recorded prevalence of 1 in 500 people among the general population [3–6], and recent studies estimating a prevalence of up to 1 in 200 people [5,7–11]. It is an important cause of disability and mortality across all ages [12], and one of the leading causes of sudden cardiac deaths among the young [13,14]. HCM is diagnosed by the presence of left ventricular hypertrophy despite the absence of any abnormal loading conditions causing it [15–18].

In the majority of cases, HCM is considered to be inherited as an autosomal dominant trait [7,19,20] and to be caused by variants in genes encoding cardiac sarcomeric proteins [7,19,21,22]. Thus far, >1400 HCM variants have been identified, of which the majority, approximately 90%, reside in the genes encoding proteins of the thin and thick filaments of the sarcomere (*MYH7*, *MYBPC3*, and *TNNT2*) [9,17,23,24]. Variants in genes *MYH7* and *MYBPC3* are the two most common factors, being together responsible for more than 50% of HCM patients with pathogenic variants [10,15,25–28]. Variants in other genes encoding sarcomeric proteins, including *TNNT2*, *TNNI3*, *TPM1*, *ACTC1*, *MYL2*, and *MYL3*, are also identified as causes of HCM [15,16,26]. Only 30–60% of patients with established clinical diagnosis of HCM carry variants in sarcomeric genes [5,22]. Up to 40% of the HCM cases do not have any known HCM variant [29]. Many non-sarcomeric genes implicated in

the disease have been progressively included in panels for HCM, despite limited evidence of a causal role in HCM [30].

Genotype–phenotype associations in HCM remain incompletely understood [31]. Structural outcomes of variants in main causative HCM genes are still unknown. Even potential cardiac regions affected by the variants are incompletely understood. Variants in *MYH7* are associated with the restrictive phenotype [3]. Variants in *MYH7* and *MYBPC3* are the most common in HCM involving basal septum [15]. Variants in *TNNT2* are associated with right atrial enlargement in HCM patients [3,32]. Gene-specific findings (structural outcomes of variants in relevant genes or cardiac regions affected by the variants) could better connect genotype and phenotype in HCM and help in the identification and clarification of HCM mechanisms. A better understanding of HCM mechanisms could lead to better treatment opportunities and finally, better outcomes for HCM patients.

Echocardiography is the primary imaging modality for establishing HCM diagnosis and for monitoring the disease, as well as for basic hemodynamic status assessment [10,33–35].

Artificial intelligence (AI) is used to study patterns in data and develop models that can make predictions. Explainable artificial intelligence methods demonstrate the relationships among such predictions [36]. Applications of AI have the potential to be useful across several medical domains [37]. Classification in AI concerns the problem of identification (prediction) regarding which groups or categories an instance belongs to [38]. Deep learning, a branch of AI, has an important role in knowledge discovery from biomedical big data [39], including cardiology [40]. Deep learning is particularly useful for image classification [41–43]. For pattern recognition tasks, deep convolutional neural networks are the most commonly used. They can extract relevant features for a given task from the training samples [44].

The aim of this study was to identify gene-specific discriminative echocardiogram findings (cardiac regions affected by the variants) in HCM, more precisely, to identify structures that AI algorithms choose to use to distinguish causal gene variant-positive HCM patients from variant-negative HCM patients. This is one of the first studies that tried to connect various echocardiographic parameters in HCM patients using AI.

2. Materials and Methods

This study involved 2 visits of 46 adult patients (≥ 18 years of age) with a confirmed diagnosis of HCM, who met the inclusion and exclusion criteria—as specified in the SILICOFCM study design [45]. Demographics; information about symptoms, signs, and comorbidities; and electrocardiographic parameters were collected as specified in the SILICOFCM study design [45].

The mean age of the HCM patients was 60.7 ± 10.3 years, and most of them were male 32 (69.6%), with a mean body mass index (BMI) of 29.0 ± 4.5 kg/m². In 5 (10.9%) patients, variants in *MYH7* were found; in 16 (34.8%) patients, variants in *MYBPC3* were found; in 6 (13.0%) patients, variants in *TNNT2* were found (Table S1); and in 8 (17.4%) patients, no variants were detected in any of the genes analyzed.

In Table 1, a description of symptoms, signs, and comorbidities of the study cohort is shown; an echocardiographic description is presented in Table 2, and an electrocardiographic description is presented in Table 3.

Table 1. Symptoms, signs, and comorbidities (all patients, $n = 46$).

	<i>n</i> (%)	Mean \pm SD
Fatigue	28 (60.9)	-
Dyspnea	17 (37.0)	-
Chest pain	15 (32.6)	-
Palpitations	12 (26.1)	-
Syncope	5 (10.9)	-
Blood pressure, systolic (mmHg)	-	132.8 \pm 21.7
Blood pressure, diastolic (mmHg)	-	74.6 \pm 10.7
Heart murmur	12 (26.1)	-
Pulmonary crackles	1 (2.2)	-
Pretibial edema	7 (15.2)	-
Diabetes mellitus	7 (15.2)	-
Thyroid disease	2 (4.3)	-
Renal dysfunction	2 (4.3)	-
Hepatic dysfunction	1 (2.2)	-
Chronic obstructive pulmonary disease	5 (10.9)	-
Anemia	2 (4.3)	-
Neuromuscular disease	1 (2.2)	-

Data are presented as n (%) for categorical variables and as mean \pm standard deviation (SD) for continuous variables.

Table 2. Echocardiography (all patients, $n = 46$).

	<i>n</i> (%)	Mean \pm SD
LA (mm)	-	41.9 \pm 5.5
LAV (mL)	-	90.6 \pm 27.3
LAV index (mL/m ²)	-	44.4 \pm 13.7
MV maxPG (mmHg)	-	4.8 \pm 2.6
MV meanPG (mmHg)	-	1.9 \pm 1.2
MVVTI (cm)	-	30.3 \pm 8.6
Systolic anterior motion	8 (17.4)	-
Papillary muscle abnormalities	1 (2.2)	-
Mitral leaflet abnormalities	5 (10.9)	-
Calcification of mitral annulus	9 (19.6)	-
IVSd (mm)	-	17.8 \pm 4.4
PLWd (mm)	-	15.6 \pm 3.5
LVIDs (mm)	-	29.8 \pm 8.0
LVIDd (mm)	-	47.5 \pm 7.1
EDVLV (mL)	-	117.4 \pm 139.3
ESVLV (mL)	-	40.1 \pm 26.9
SVLV (mL)	-	57.8 \pm 20.5
EFLV (%)	-	61.9 \pm 9.7
Myocardial fibrosis	0 (0.0)	-
Hypokinesia	4 (8.7)	-
Akinesia	1 (2.2)	-
Dyskinesia	0 (0.0)	-
Hyperkinesia	0 (0.0)	-
E/E'	-	15.9 \pm 7.3
Diastolic dysfunction grade	-	1.2 \pm 0.7
AV maxPG (mmHg)	-	14.8 \pm 9.9
AV meanPG (mmHg)	-	7.7 \pm 5.2
AVVTI (cm)	-	37.6 \pm 13.9
AO (mm)	-	22.4 \pm 2.8
AOvs (mm)	-	17.6 \pm 3.0

Table 2. *Cont.*

	<i>n</i> (%)	Mean \pm SD
AscAO (mm)	-	33.5 \pm 4.9
RAVs (mL)	-	48.3 \pm 18.5
TAPSE (mm)	-	22.0 \pm 4.0
RVSP (mmHg)	-	37.7 \pm 12.4

Data are presented as *n* (%) for categorical variables and as mean \pm SD for continuous variables. LA—left atrial diameter, LAV—left atrial volume, MVmaxPG—transmitral maximal pressure gradient, MVmeanPG—transmitral mean pressure gradient, MVVTI—mitral valve velocity–time integral, IVSd—interventricular septum thickness, PLWd—posterior left ventricle wall thickness at end-diastole, LVIDs—left ventricular internal dimension at end-systole, LVIDd—left ventricular internal dimension at end-diastole, EDVLV—end-diastolic volume of the left ventricle, ESVLV—end-systolic volume of left ventricle, SVLV—stroke volume of the left ventricle, EFLV—left ventricular ejection fraction, E/E'—ratio of peak velocity of early-diastolic transmitral flow to peak velocity of early-diastolic mitral annular motion as determined using pulsed-wave Doppler, AV maxPG—aortic valve peak pressure gradient, AV meanPG—aortic valve mean pressure gradient, AVVTI—aortic valvular velocity–time integral, AO—aortic root diameter, AOvs—aortic leaflet separation diameter, AscAO—diameter of ascending aorta, RAVs—right atrial volume at end-systole, TAPSE—tricuspid annular plane systolic excursion, RVSP—right ventricle systolic pressure.

Table 3. Electrocardiography (all patients, *n* = 46).

	<i>n</i> (%)	Mean \pm SD
Sinus rhythm	38 (82.6)	-
Atrial flutter	0 (0.0)	-
Atrial fibrillation	6 (13.0)	-
Paroxysmal supraventricular tachycardia	1 (2.2)	-
Non-sustained ventricular tachycardia	5 (10.9)	-
Pacemaker	3 (6.5)	-
Heart rate (bpm)	-	65.2 \pm 11.0
Atrioventricular block I	2 (4.3)	-
Atrioventricular block II (Mobitz 1)	1 (2.2)	-
Atrioventricular block II (Mobitz 2)	1 (2.2)	-
Atrioventricular block III	0 (0.0)	-
Left bundle branch block	3 (6.5)	-
Right bundle branch block	5 (10.9)	-
Left anterior hemiblock	3 (6.5)	-
Right anterior hemiblock	0 (0.0)	-
PR interval (ms)	-	169.5 \pm 33.4
QRS duration (ms)	-	106.5 \pm 26.9
Sokolow index (mm)	-	25.2 \pm 9.8
Significant Q wave	5 (10.9)	-
ST segment abnormalities	18 (39.1)	-
Negative T wave	33 (71.7)	-

Data are presented as *n* (%) for categorical variables and as mean \pm SD for continuous variables.

2.1. Genetic Testing

After the isolation of DNA from the whole blood of patients using a QIAamp DNA Blood BioRobot MDx kit (QIAGEN GmbH, Hilden, Germany), 174 genes were analyzed on the Next Generation Sequencing platform (Illumina, Inc., San Diego, CA, USA) using the TruSight Cardio Sequencing Panel (Illumina, Inc., San Diego, CA, USA) for the identification of causal variants implicated in inherited cardiac conditions. Only patients with detected variants in *MYH7*, *MYBPC3*, or *TNNT2*, as well as patients without detected variants were included in the further analysis. Other patients were excluded because of a small number of detected variants in other causal genes and the potential bias that it would bring to final results (Table S1).

2.2. Ultrasonic Records

A transthoracic echocardiography was performed. Echocardiograms were recorded in two patient visits, in real-time, during 3 cardiac cycles in the standard parasternal (long-axis) and apical views (apical 4 and apical 2).

2.3. Identification of Gene-Specific Discriminative Echocardiogram Findings

Ultrasonic records in DICOM format were converted into JPG images using RadiAnt DICOM Viewer v. 2021.2.2. Images were grouped based on the views they represented: in parasternal long-axis, apical 2-chamber, and apical 4-chamber groups. Ultrasonic images showing the beginning of a P-wave and a T-wave on electrocardiogram (ECG) (as representative images of ventricular diastole and ventricular systole) were detached, each to a separate image batch. In order to remove background noise (patient details, date, heart rate, ECG, etc.), a custom masker was used. The masker was built using the Python OpenCV library. Masked ultrasonic images, showing only the region of interest, were used for further analysis (Figure 1).

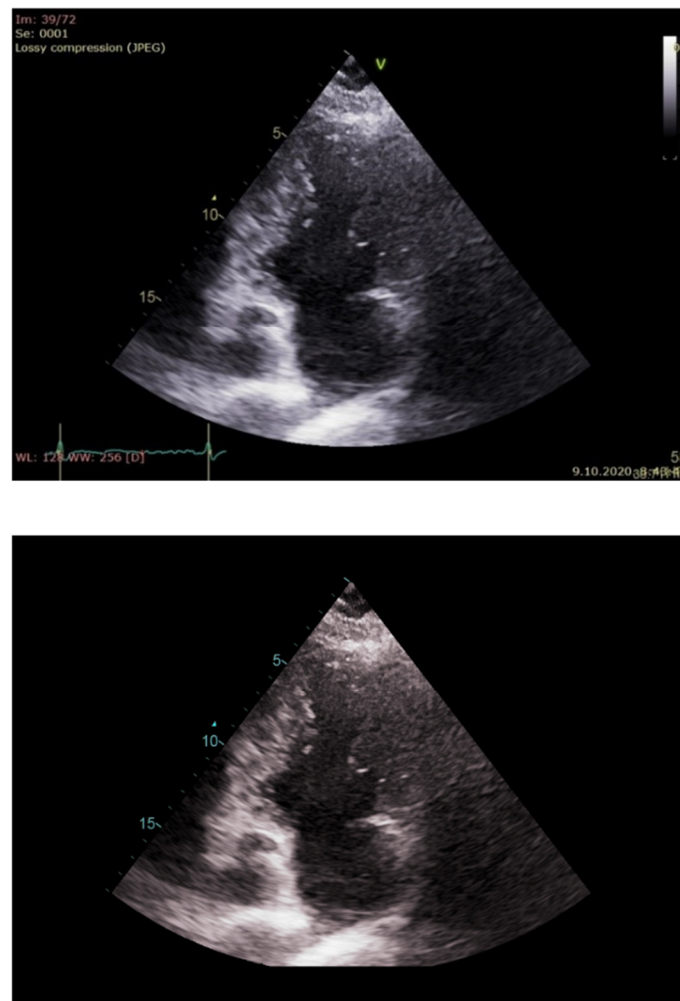


Figure 1. Same ultrasonic image before (**up**) and after (**down**) custom masker application.

Gene-specific discriminative echocardiogram findings were identified using the computer vision library Fast AI. This was accomplished with the generation of deep learning models for the classification of ultrasonic images based on the underlying genotype (variant in *MYH7* vs. variant not detected; variant in *MYBPC3* vs. variant not detected; and variant in *TNNT2* vs. variant not detected) and later analysis and interpretation of the most decisive image regions (which most directed the prediction of the model toward one class or another). Training and test sets were split manually using the holdout method. Images obtained in two visits for each patient were both assigned to either train or test set only [46]. Models were built using the following setting: image_size = 224, batch_size = 4, without data augmentation, using pre-trained ResNet18. The most discriminative areas for classification were assessed using plot_top_losses and heatmaps (heatmap = True). When

heatmap = True, Grad-CAM heatmaps [47] are overlaid on each image. The heatmaps highlight the regions in an image that the model focuses on while trying to make a prediction (the deeper the highlighted color, the more relevant the region is for a particular class prediction).

3. Results

Models for echocardiographic images classification of patients with a variant in the *MYH7* gene and those without a detected variant; patients with a variant in the *MYBPC3* gene and those without a detected variant; as well as patients with a variant in the *TNNT2* gene and those without detected a variant were created (Table 4). The discriminative areas for the classification of a given image (areas that contributed the most to the decision for the classification) are shown in Table 4 and Figures 2–19 (the deeper the highlighted color, the more relevant the region is for a particular class prediction). Echocardiographic and electrocardiographic descriptions are shown in Tables 5–10.

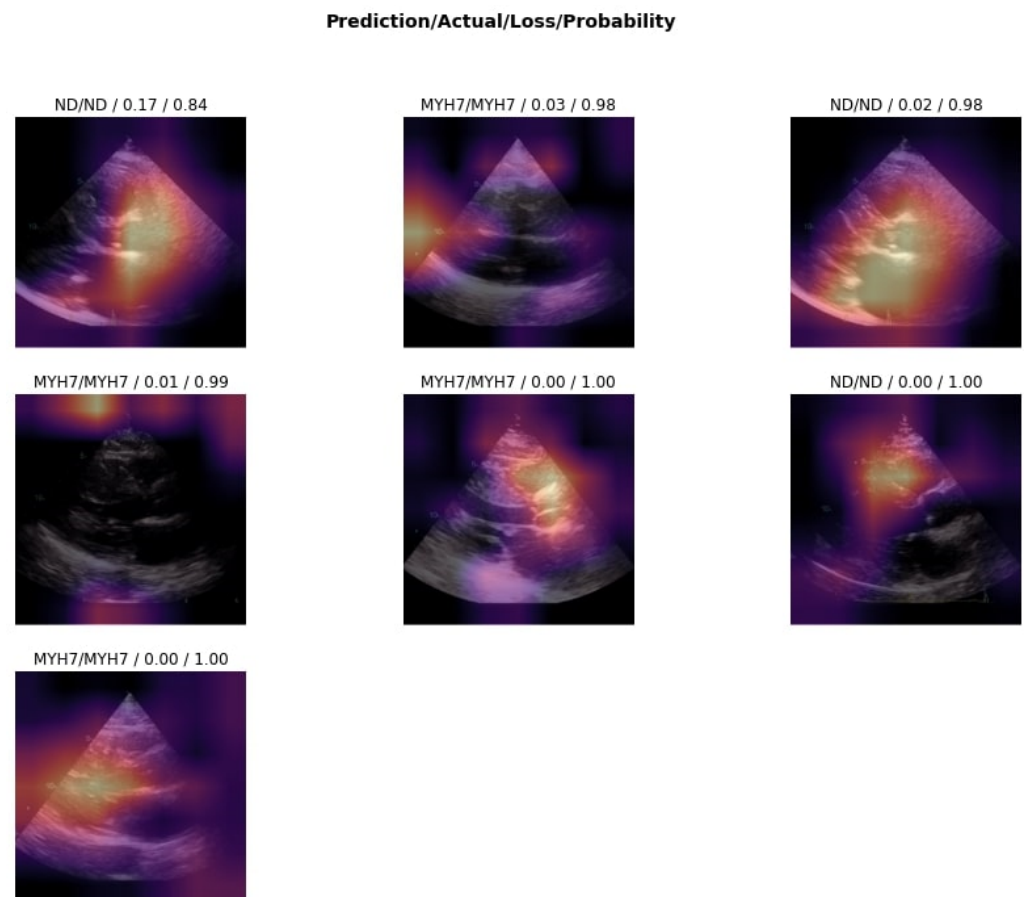


Figure 2. Discriminative areas for classification of a given image (variant in *MYH7* vs. variant not detected), parasternal long-axis view during ventricular diastole. The deeper the highlighted color, the more relevant the region is for a particular class prediction.

Table 4. Gene-specific discriminative echocardiogram findings.

Mutated Gene	Discriminative Structure (Mutated Gene vs. Variant Not Detected)	View	Cardiac Cycle Phase	Performance
MYH7	septum and LVOT segment (Figure 2)	parasternal long axis	ventricular diastole	accuracy = 1.000, precision = 1.000, recall = 1.000
	anterior wall and apex (Figure 3)		ventricular systole	accuracy = 1.000, precision = 1.000, recall = 1.000
	none (Figure 4)	apical two-chamber	ventricular diastole	accuracy = 0.928, precision = 1.000, recall = 0.875
	none (Figure 5)		ventricular systole	accuracy = 1.000, precision = 1.000, recall = 1.000
	right ventricle (Figure 6)	apical four-chamber	ventricular diastole	accuracy = 1.000, precision = 1.000, recall = 1.000
	mitral apparatus (Figure 7)		ventricular systole	accuracy = 1.000, precision = 1.000, recall = 1.000
	MYBPC3	none (Figure 8)	parasternal long axis	ventricular diastole
left ventricle/chamber (Figure 9)		ventricular systole		accuracy = 1.000, precision = 1.000, recall = 1.000
left ventricle (Figure 10)		apical two-chamber	ventricular diastole	accuracy = 1.000, precision = 1.000, recall = 1.000
none (Figure 11)			ventricular systole	accuracy = 0.947, precision = 1.000, recall = 0.917
septum (Figure 12)		apical four-chamber	ventricular diastole	accuracy = 0.969, precision = 0.941, recall = 1.000
septum (Figure 13)			ventricular systole	accuracy = 1.000, precision = 1.000, recall = 1.000
TNNT2		none (Figure 14)	parasternal long axis	ventricular diastole
	none (Figure 15)	ventricular systole		accuracy = 1.000, precision = 1.000, recall = 1.000
	septum (Figure 16)	apical two-chamber	ventricular diastole	accuracy = 1.000, precision = 1.000, recall = 1.000
	septum (Figure 17)		ventricular systole	accuracy = 0.909, precision = 1.000, recall = 0.750
	septum (Figure 18)	apical four-chamber	ventricular diastole	accuracy = 1.000, precision = 1.000, recall = 1.000
	septum and right ventricle (Figure 19)		ventricular systole	accuracy = 1.000, precision = 1.000, recall = 1.000

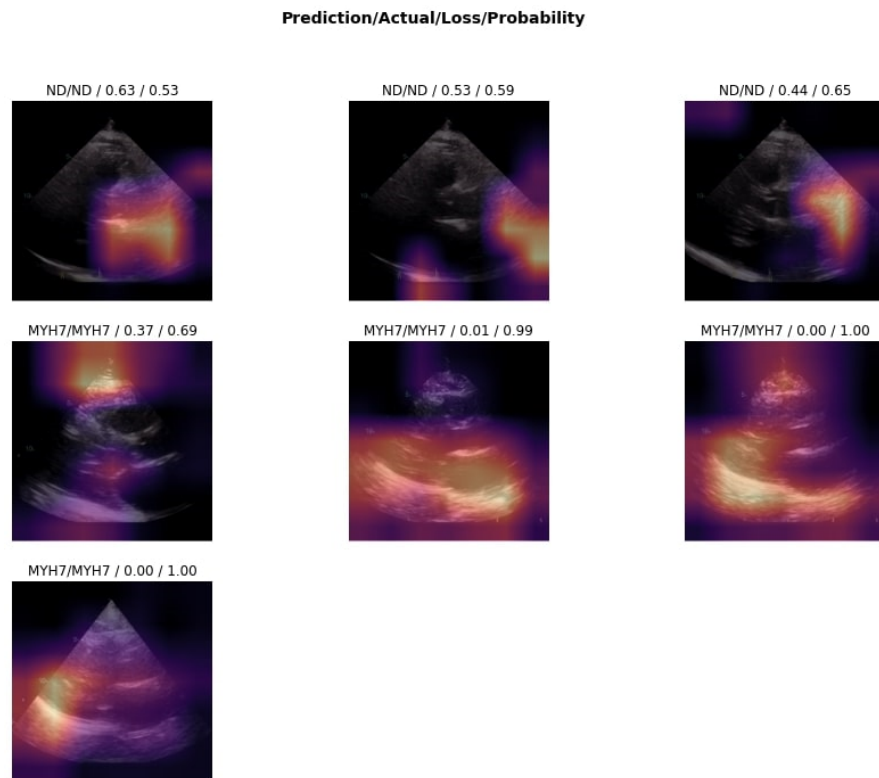


Figure 3. Discriminative areas for classification of a given image (variant in *MYH7* vs. variant not detected), parasternal long-axis view during ventricular systole. The deeper the highlighted color, the more relevant the region is for a particular class prediction.

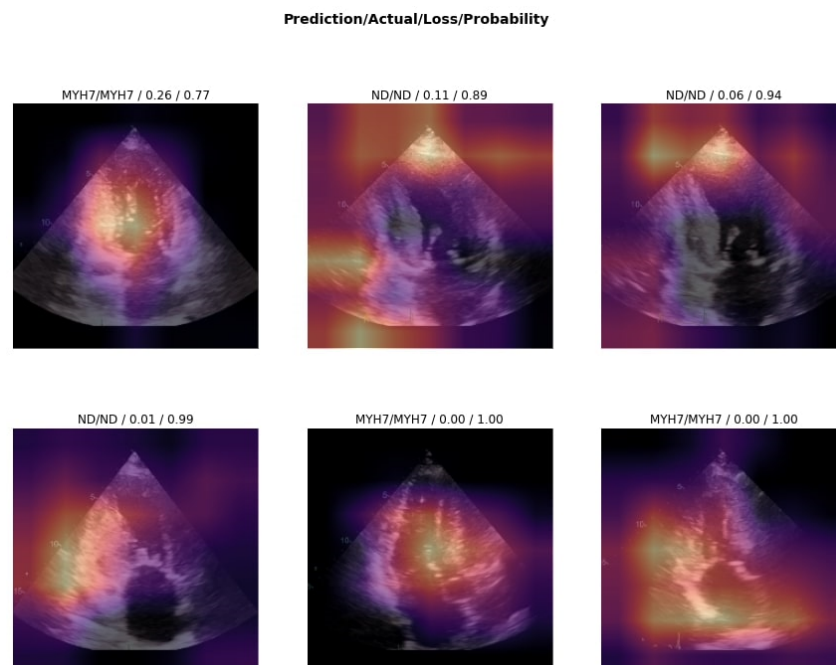


Figure 4. Discriminative areas for classification of a given image (variant in *MYH7* vs. variant not detected), apical 2-chamber view during ventricular diastole. The deeper the highlighted color, the more relevant the region is for a particular class prediction.

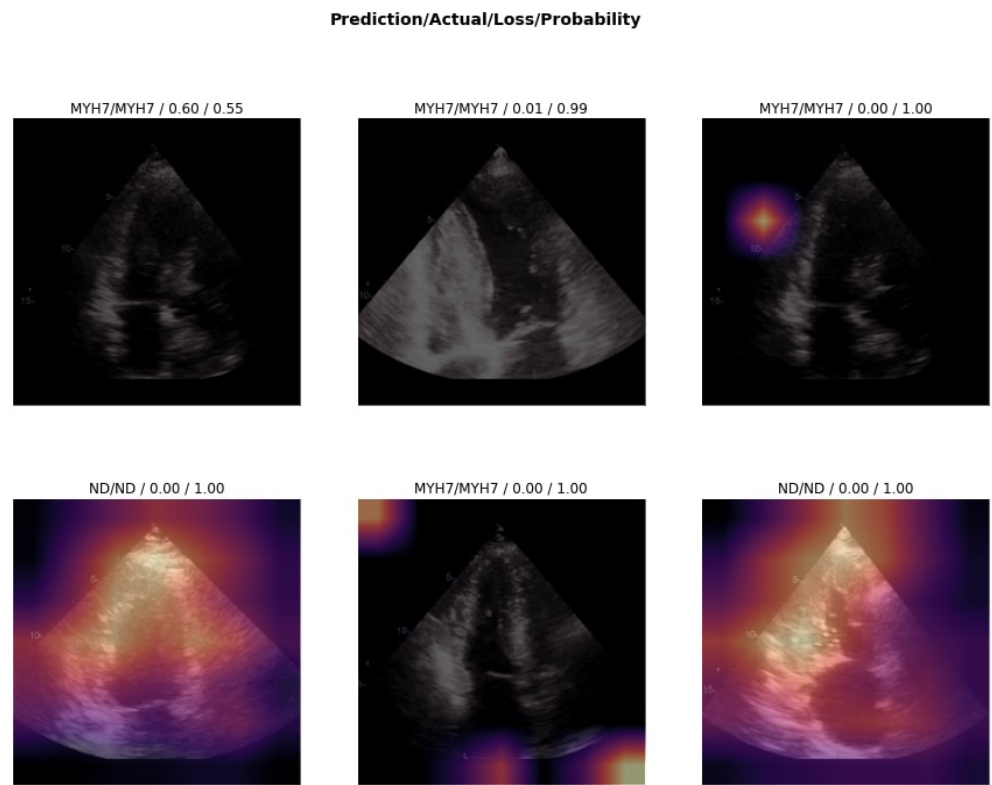


Figure 5. Discriminative areas for classification of a given image (variant in *MYH7* vs. variant not detected), apical 2-chamber view during ventricular systole. The deeper the highlighted color, the more relevant the region is for a particular class prediction.

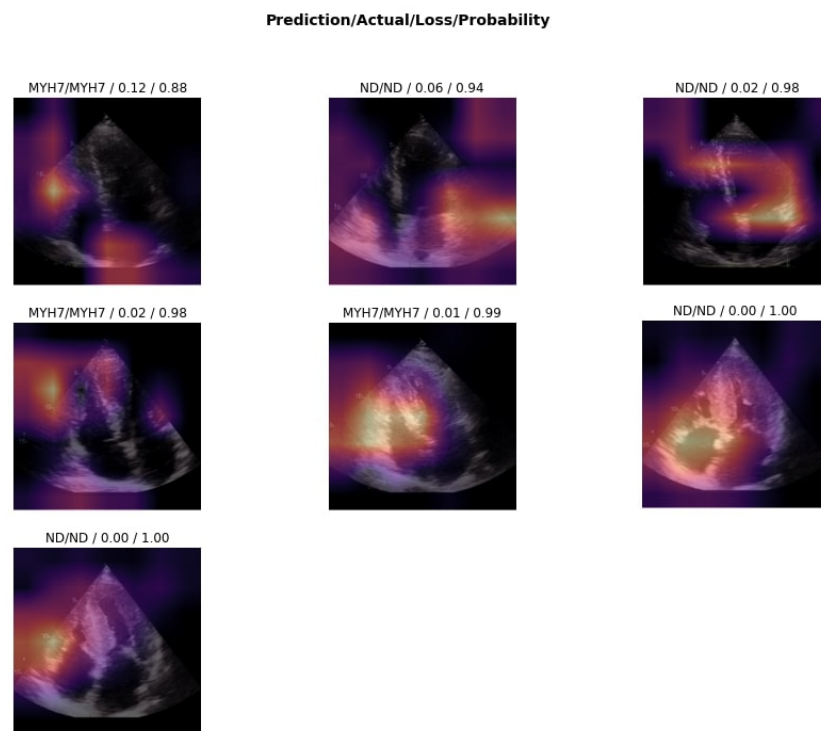


Figure 6. Discriminative areas for classification of a given image (variant in *MYH7* vs. variant not detected), apical 4-chamber view during ventricular diastole. The deeper the highlighted color, the more relevant the region is for a particular class prediction.

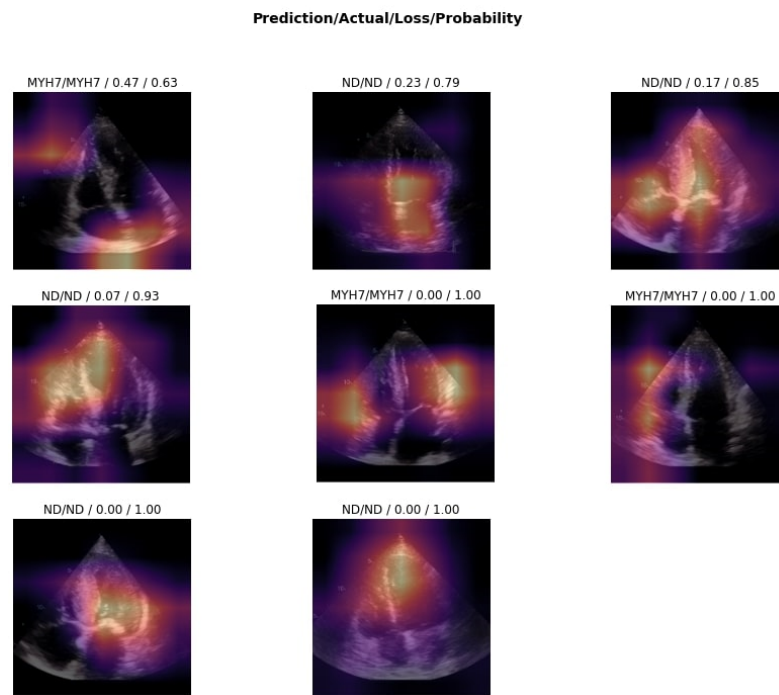


Figure 7. Discriminative areas for classification of a given image (variant in *MYH7* vs. variant not detected), apical 4-chamber view during ventricular systole. The deeper the highlighted color, the more relevant the region is for a particular class prediction.

Table 5. Echocardiography (variant in *MYH7* vs. variant not detected).

	<i>MYH7</i>	Not Detected	<i>p</i> -Value
LA (mm)	41.0 ± 5.2	43.5 ± 6.3	0.478
LAV (mL)	88.4 ± 23.5	90.9 ± 25.2	0.863
LAV index (mL/m ²)	45.2 ± 10.0	44.1 ± 11.1	0.851
MV maxPG (mmHg)	3.7 ± 1.3	4.1 ± 1.3	0.672
MV meanPG (mmHg)	1.4 ± 0.5	2.2 ± 1.6	0.212
MVVTI (cm)	30.6 ± 8.7	30.6 ± 10.0	0.996
Systolic anterior motion	1 (20.0)	2 (25.0)	0.835
Papillary muscle abnormalities	0 (0.0)	1 (12.5)	0.411
Mitral leaflet abnormalities	0 (0.0)	0 (0.0)	-
Calcification of mitral annulus	0 (0.0)	4 (50.0)	0.057
IVSd (mm)	16.2 ± 3.3	18.9 ± 4.6	0.287
PLWd (mm)	17.6 ± 8.3	15.8 ± 4.2	0.941
LVIDs (mm)	30.2 ± 6.1	30.6 ± 10.7	0.937
LVIDd (mm)	46.2 ± 4.8	47.9 ± 9.4	0.722
EDVLV (mL)	84.2 ± 25.2	97.3 ± 37.4	0.509
ESVLV (mL)	24.7 ± 8.9	41.7 ± 24.8	0.174
SVLV (mL)	59.5 ± 19.6	55.6 ± 16.7	0.705
EFLV (%)	70.4 ± 7.0	59.3 ± 10.2	0.056
Myocardial fibrosis	0 (0.0)	0 (0.0)	-
Hypokinesia	0 (0.0)	1 (12.5)	0.411
Akinesia	0 (0.0)	0 (0.0)	-
Dyskinesia	0 (0.0)	0 (0.0)	-
Hyperkinesia	0 (0.0)	0 (0.0)	-

Table 5. *Cont.*

	<i>MYH7</i>	Not Detected	<i>p</i> -Value
E/E'	13.3 ± 4.6	21.6 ± 12.5	0.239
Diastolic dysfunction grade	1.3 ± 0.6	1.5 ± 2.1	0.869
AV maxPG (mmHg)	16.3 ± 16.1	15.9 ± 11.0	0.833
AV meanPG (mmHg)	8.3 ± 7.8	8.2 ± 5.4	0.607
AVVTI (cm)	38.2 ± 15.0	43.7 ± 17.2	0.569
AO (mm)	22.4 ± 3.0	22.1 ± 2.2	0.852
AOvs (mm)	19.2 ± 2.3	17.3 ± 3.3	0.272
AscAO (mm)	30.8 ± 4.0	31.4 ± 2.4	0.737
RAVs (mL)	45.6 ± 15.6	40.0 ± 13.8	0.592
TAPSE (mm)	24.6 ± 3.0	19.9 ± 3.3	0.028 *
RVSP (mmHg)	33.0 ± 5.2	39.3 ± 15.5	0.260

Data are presented as *n* (%) for categorical variables and as mean ± SD for continuous variables. LA—left atrial diameter, LAV—left atrial volume, MVmaxPG—transmitral maximal pressure gradient, MVmeanPG—transmitral mean pressure gradient, MVVTI—mitral valve velocity–time integral, IVSd—interventricular septum thickness, PLWd—posterior left ventricle wall thickness at end-diastole, LVIDs—left ventricular internal dimension at end-systole, LVIDd—left ventricular internal dimension at end-diastole, EDVLV—end-diastolic volume of the left ventricle, ESVLV—end-systolic volume of left ventricle, SVLV—stroke volume of the left ventricle, EFLV—left ventricular ejection fraction, E/E'—ratio of peak velocity of early-diastolic transmitral flow to peak velocity of early-diastolic mitral annular motion as determined using pulsed-wave Doppler, AV maxPG—aortic valve peak pressure gradient, AV meanPG—aortic valve mean pressure gradient, AVVTI—aortic valvular velocity–time integral, AO—aortic root diameter, AOvs—aortic leaflet separation diameter, AscAO—diameter of ascending aorta, RAVs—right atrial volume at end-systole, TAPSE—tricuspid annular plane systolic excursion, RVSP—right ventricle systolic pressure, *—statistically significant.

Table 6. Electrocardiography (variant in *MYH7* vs. variant not detected).

	<i>MYH7</i>	Not Detected	<i>p</i> -Value
Sinus rhythm	5 (100.0)	8 (100.0)	-
Atrial flutter	0 (0.0)	0 (0.0)	-
Atrial fibrillation	0 (0.0)	0 (0.0)	-
Paroxysmal supraventricular tachycardia	0 (0.0)	1 (12.5)	0.411
Non-sustained ventricular tachycardia	0 (0.0)	0 (0.0)	-
Pacemaker	0 (0.0)	0 (0.0)	-
Heart rate (bpm)	59.0 ± 9.1	62.7 ± 5.2	0.106
Atrioventricular block I	0 (0.0)	0 (0.0)	-
Atrioventricular block II (Mobitz 1)	0 (0.0)	0 (0.0)	-
Atrioventricular block II (Mobitz 2)	0 (0.0)	0 (0.0)	-
Atrioventricular block III	0 (0.0)	0 (0.0)	-
Left bundle branch block	1 (0.2)	1 (12.5)	0.715
Right bundle branch block	2 (0.4)	0 (0.0)	0.052
Left anterior hemiblock	0 (0.0)	1 (12.5)	0.411
Right anterior hemiblock	0 (0.0)	0 (0.0)	-
PR interval (ms)	157.4 ± 28.7	170.5 ± 23.6	0.388
QRS duration (ms)	123.0 ± 34.8	96.1 ± 17.9	0.090
Sokolow index (mm)	26.2 ± 9.4	26.9 ± 13.1	0.941
Significant Q wave	0 (0.0)	2 (25.0)	0.224
ST segment abnormalities	1 (20.0)	6 (75.0)	0.053
Negative T wave	5 (100.0)	7 (87.5)	0.411

Data are presented as *n* (%) for categorical variables and as mean ± SD for continuous variables.

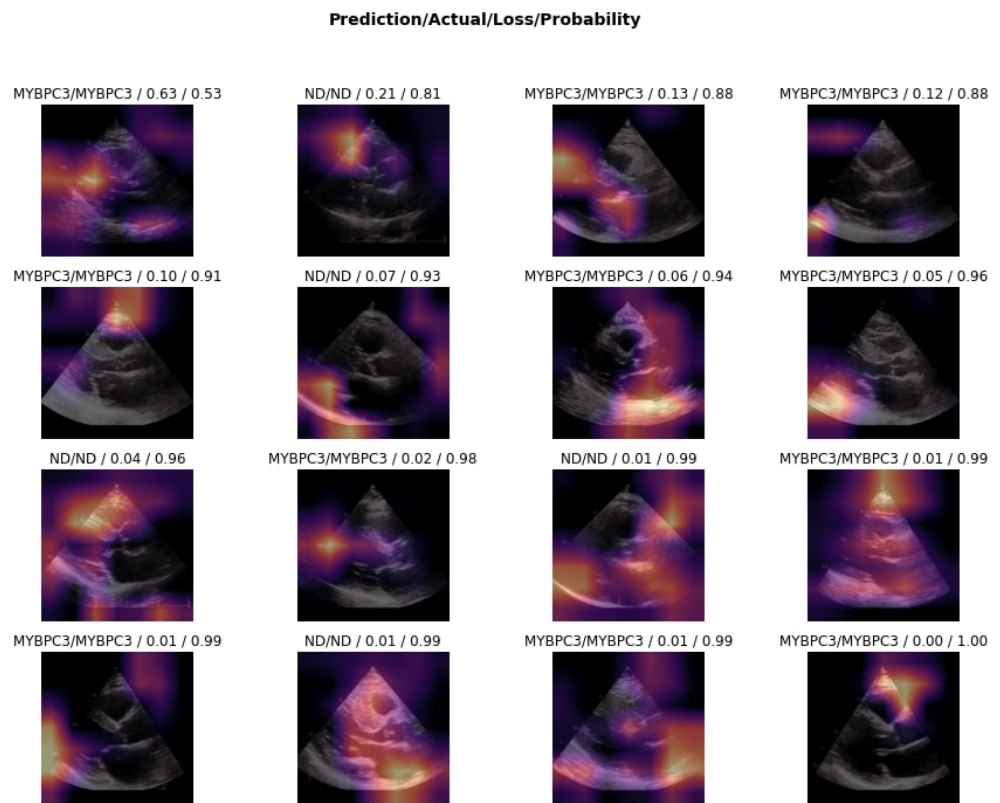


Figure 8. Discriminative areas for classification of a given image (variant in *MYBPC3* vs. variant not detected), parasternal long-axis view during ventricular diastole. The deeper the highlighted color, the more relevant the region is for a particular class prediction.

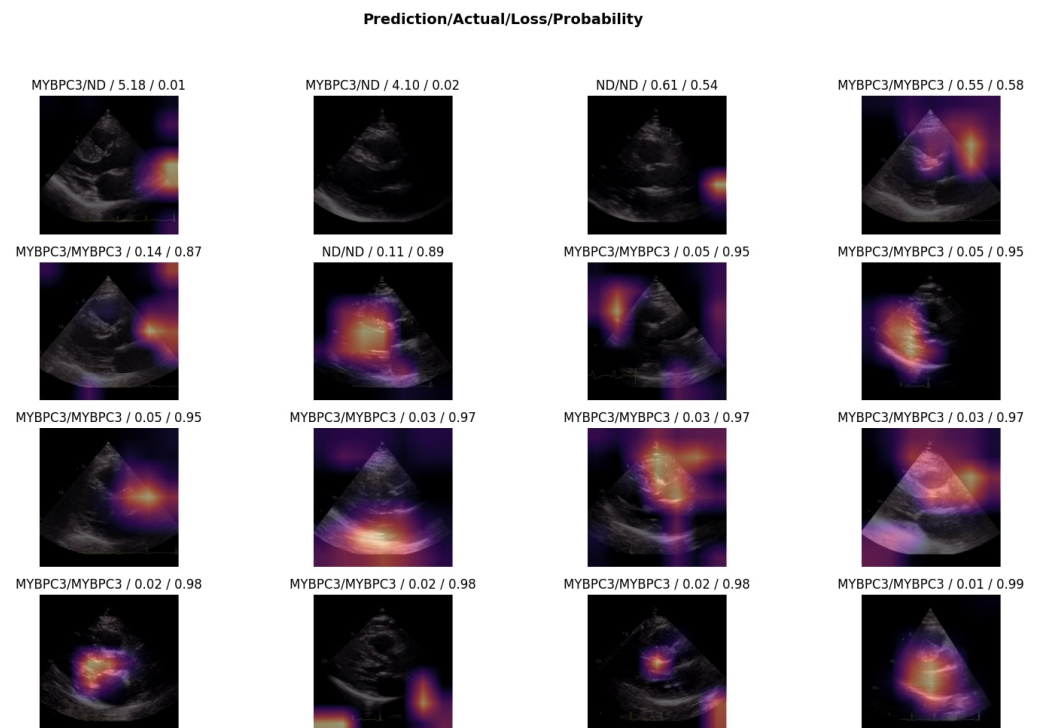


Figure 9. Discriminative areas for classification of a given image (variant in *MYBPC3* vs. variant not detected), parasternal long-axis view during ventricular systole. The deeper the highlighted color, the more relevant the region is for a particular class prediction.

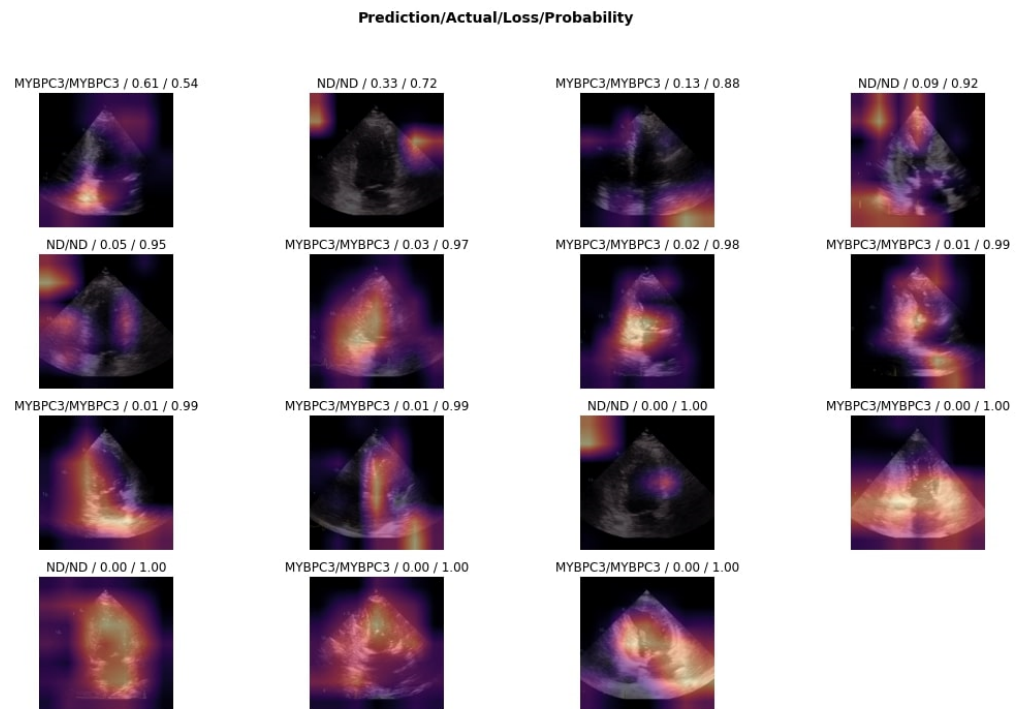


Figure 10. Discriminative areas for classification of a given image (variant in *MYBPC3* vs. variant not detected), apical 2-chamber view during ventricular diastole. The deeper the highlighted color, the more relevant the region is for a particular class prediction.

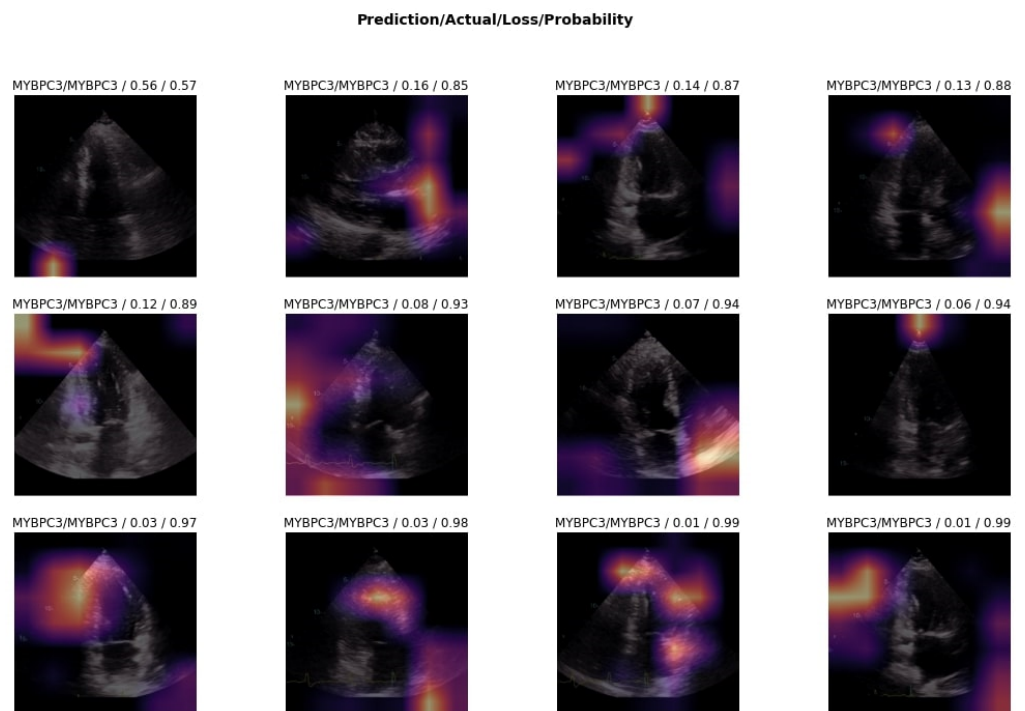


Figure 11. Discriminative areas for classification of a given image (variant in *MYBPC3* vs. variant not detected), apical 2-chamber view during ventricular systole. The deeper the highlighted color, the more relevant the region is for a particular class prediction.

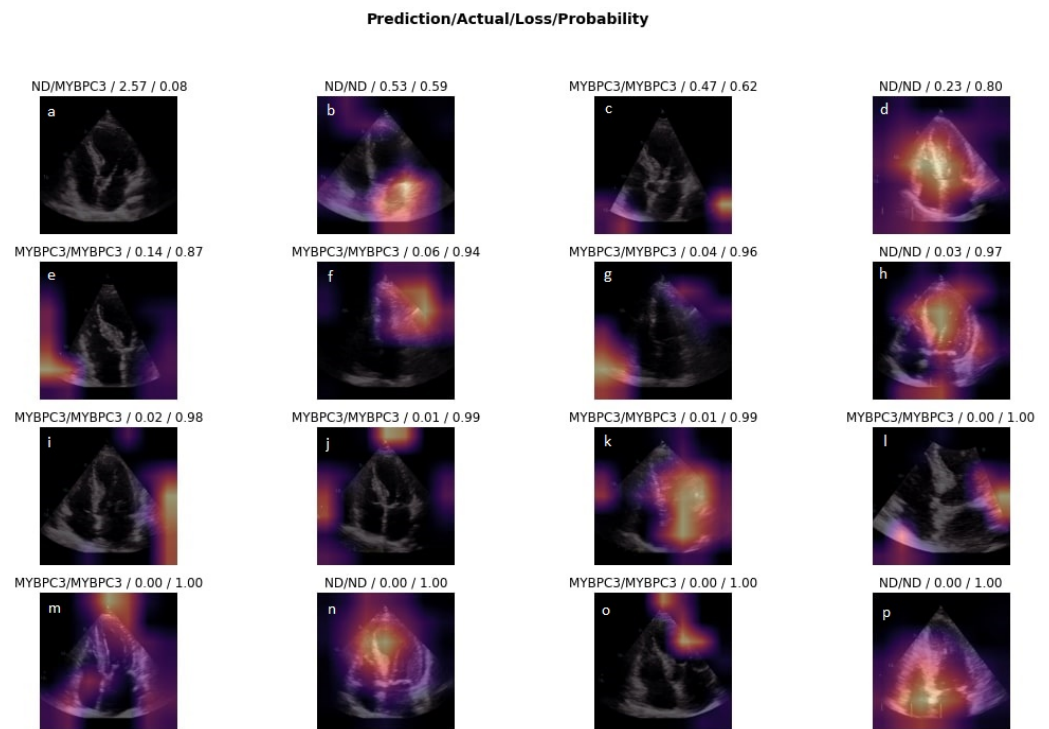


Figure 12. Discriminative areas for classification of a given image (variant in *MYBPC3* vs. variant not detected), apical 4-chamber view during ventricular diastole. The deeper the highlighted color, the more relevant the region is for a particular class prediction.

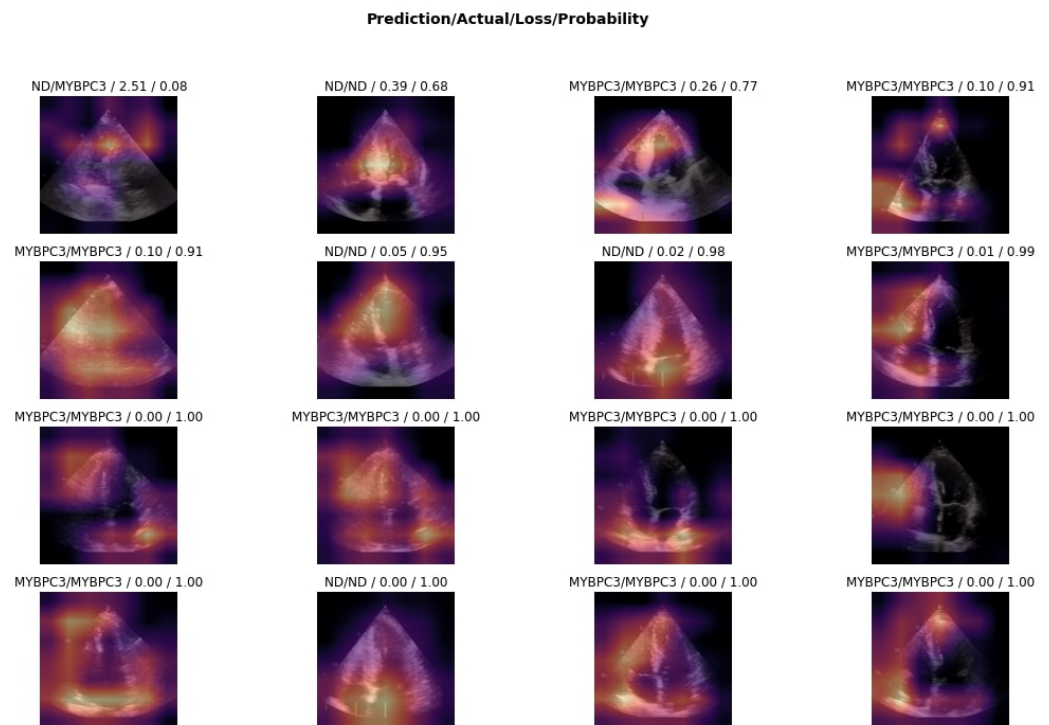


Figure 13. Discriminative areas for classification of a given image (variant in *MYBPC3* vs. variant not detected), apical 4-chamber view during ventricular systole. The deeper the highlighted color, the more relevant the region is for a particular class prediction.

Table 7. Echocardiography (variant in *MYBPC3* vs. variant not detected).

	<i>MYBPC3</i>	Not Detected	<i>p</i> -Value
LA (mm)	41.4 ± 4.3	43.5 ± 6.3	0.324
LAV (mL)	81.9 ± 18.5	90.9 ± 25.2	0.333
LAV index (mL/m ²)	39.8 ± 7.7	44.1 ± 11.1	0.282
MV maxPG (mmHg)	5.6 ± 2.4	4.1 ± 1.3	0.111
MV meanPG (mmHg)	2.3 ± 1.4	2.2 ± 1.6	0.902
MVVTI (cm)	29.7 ± 8.5	30.6 ± 10.0	0.824
Systolic anterior motion	3 (18.7)	2 (25.0)	0.722
Papillary muscle abnormalities	0 (0.0)	1 (12.5)	0.149
Mitral leaflet abnormalities	2 (12.5)	0 (0.0)	0.296
Calcification of mitral annulus	1 (6.25)	4 (50.0)	0.013 *
IVSd (mm)	17.0 ± 3.1	18.9 ± 4.6	0.326
PLWd (mm)	14.6 ± 2.1	15.8 ± 4.2	0.471
LVIDs (mm)	30.0 ± 7.5	30.6 ± 10.7	0.869
LVIDd (mm)	47.3 ± 6.0	47.9 ± 9.4	0.845
EDVLV (mL)	87.9 ± 32.1	97.3 ± 37.4	0.530
ESVLV (mL)	32.8 ± 18.9	41.7 ± 24.8	0.338
SVLV (mL)	55.1 ± 17.8	55.6 ± 16.7	0.949
EFLV (%)	65.1 ± 8.5	59.3 ± 10.2	0.149
Myocardial fibrosis	0 (0.0)	0 (0.0)	-
Hypokinesia	1 (6.25)	1 (12.5)	0.602
Akinesia	0 (0.0)	0 (0.0)	-
Dyskinesia	0 (0.0)	0 (0.0)	-
Hyperkinesia	0 (0.0)	0 (0.0)	-
E/E'	13.8 ± 3.6	21.6 ± 12.5	0.153
Diastolic dysfunction grade	1.2 ± 0.6	1.5 ± 2.1	0.544
AV maxPG (mmHg)	16.5 ± 10.8	15.9 ± 11.0	0.854
AV meanPG (mmHg)	8.7 ± 5.4	8.2 ± 5.5	0.759
AVVTI (cm)	38.9 ± 14.2	43.7 ± 17.2	0.476
AO (mm)	22.2 ± 2.3	22.1 ± 2.2	0.950
AOvs (mm)	16.9 ± 3.3	17.3 ± 3.3	0.793
AscAO (mm)	33.1 ± 5.4	31.4 ± 2.4	0.339
RAVs (mL)	44.0 ± 15.9	40.0 ± 13.8	0.678
TAPSE (mm)	22.7 ± 3.8	20.0 ± 3.3	0.108
RVSP (mmHg)	34.9 ± 12.5	39.0 ± 15.5	0.488

Data are presented as *n* (%) for categorical variables and as mean ± SD for continuous variables. LA—left atrial diameter, LAV—left atrial volume, MVmaxPG—transmitral maximal pressure gradient, MVmeanPG—transmitral mean pressure gradient, MVVTI—mitral valve velocity–time integral, IVSd—interventricular septum thickness, PLWd—posterior left ventricle wall thickness at end-diastole, LVIDs—left ventricular internal dimension at end-systole, LVIDd—left ventricular internal dimension at end-diastole, EDVLV—end-diastolic volume of the left ventricle, ESVLV—end-systolic volume of left ventricle, SVLV—stroke volume of the left ventricle, EFLV—left ventricular ejection fraction, E/E'—ratio of peak velocity of early-diastolic transmitral flow to peak velocity of early-diastolic mitral annular motion as determined using pulsed-wave Doppler, AV maxPG—aortic valve peak pressure gradient, AV meanPG—aortic valve mean pressure gradient, AVVTI—aortic valvular velocity–time integral, AO—aortic root diameter, AOvs—aortic leaflet separation diameter, AscAO—diameter of ascending aorta, RAVs—right atrial volume at end-systole, TAPSE—tricuspid annular plane systolic excursion, RVSP—right ventricle systolic pressure, *—statistically significant.

Table 8. Electrocardiography (variant in *MYBPC3* vs. variant not detected).

	<i>MYBPC3</i>	Not Detected	<i>p</i> -Value
Sinus rhythm	14 (90.0)	8 (100.0)	0.296
Atrial flutter	0 (0.0)	0 (0.0)	-
Atrial fibrillation	2 (12.5)	0 (0.0)	0.296
Paroxysmal supraventricular tachycardia	0 (0.0)	1 (12.5)	0.149
Non-sustained ventricular tachycardia	3 (18.7)	0 (0.0)	0.190
Pacemaker	0 (0.0)	0 (0.0)	-
Heart rate (bpm)	70.0 ± 12.6	62.7 ± 5.2	0.060
Atrioventricular block I	0 (0.0)	0 (0.0)	-

Table 8. Cont.

	MYBPC3	Not Detected	p-Value
Atrioventricular block II (Mobitz 1)	1 (6.25)	0 (0.0)	0.470
Atrioventricular block II (Mobitz 2)	0 (0.0)	0 (0.0)	-
Atrioventricular block III	0 (0.0)	0 (0.0)	-
Left bundle branch block	2 (12.5)	1 (12.5)	1.000
Right bundle branch block	1 (6.25)	0 (0.0)	0.470
Left anterior hemiblock	0 (0.0)	1 (12.5)	0.149
Right anterior hemiblock	0 (0.0)	0 (0.0)	-
PR interval (ms)	160.5 ± 13.9	170.5 ± 23.6	0.396
QRS duration (ms)	116.8 ± 31.9	96.1 ± 17.9	0.105
Sokolow index (mm)	24.7 ± 6.5	26.9 ± 13.1	0.945
Significant Q wave	2 (12.5)	2 (25.0)	0.439
ST segment abnormalities	5 (31.25)	6 (75.0)	0.043 *
Negative T wave	11 (68.75)	7 (87.5)	0.317

Data are presented as *n* (%) for categorical variables and as mean ± SD for continuous variables. *—statistically significant.

Table 9. Echocardiography (variant in *TNNT2* vs. variant not detected).

	TNNT2	Not Detected	p-Value
LA (mm)	41.5 ± 5.6	43.5 ± 6.3	0.552
LAV (mL)	89.8 ± 21.3	90.9 ± 25.2	0.936
LAV index (mL/m ²)	46.3 ± 11.3	44.1 ± 11.1	0.720
MV maxPG (mmHg)	4.1 ± 2.3	4.1 ± 1.3	0.942
MV meanPG (mmHg)	1.5 ± 1.1	2.2 ± 1.6	0.365
MVVTI (cm)	25.0 ± 10.5	30.6 ± 10.0	0.327
Systolic anterior motion	1 (16.7)	2 (25.0)	0.707
Papillary muscle abnormalities	0 (0.0)	1 (12.5)	0.369
Mitral leaflet abnormalities	1 (16.7)	0 (0.0)	0.231
Calcification of mitral annulus	0 (0.0)	4 (50.0)	0.040 *
IVSd (mm)	16.3 ± 6.1	18.9 ± 4.6	0.393
PLWd (mm)	16.7 ± 7.6	15.8 ± 4.2	0.845
LVIDs (mm)	26.7 ± 5.0	30.6 ± 10.7	0.420
LVIDd (mm)	44.3 ± 5.0	47.9 ± 9.4	0.422
EDVLV (mL)	67.5 ± 21.3	97.3 ± 37.4	0.108
ESVLV (mL)	22.7 ± 14.6	41.7 ± 24.8	0.029 *
SVLV (mL)	44.8 ± 13.5	55.6 ± 16.7	0.222
EFLV (%)	68.3 ± 9.9	59.3 ± 10.2	0.120
Myocardial fibrosis	0 (0.0)	0 (0.0)	-
Hypokinesia	0 (0.0)	1 (12.5)	0.369
Akinesia	0 (0.0)	0 (0.0)	-
Dyskinesia	0 (0.0)	0 (0.0)	-
Hyperkinesia	0 (0.0)	0 (0.0)	-
E/E'	14.9 ± 4.2	21.6 ± 12.5	0.275
Diastolic dysfunction grade	1.0 ± 0.0	1.5 ± 2.1	0.884
AV maxPG (mmHg)	12.4 ± 10.0	15.9 ± 11.0	0.573
AV meanPG (mmHg)	7.0 ± 6.1	8.2 ± 5.4	0.366
AVVTI (cm)	36.3 ± 18.6	43.7 ± 17.2	0.330
AO (mm)	21.3 ± 2.2	22.1 ± 2.2	0.511
AOvs (mm)	17.8 ± 3.7	17.3 ± 3.3	0.761
AscAO (mm)	34.0 ± 6.3	31.4 ± 2.4	0.340

Table 9. *Cont.*

	<i>TNNT2</i>	Not Detected	<i>p</i> -Value
RAVs (mL)	45.6 ± 6.6	40.0 ± 13.8	0.446
TAPSE (mm)	23.5 ± 3.6	20.0 ± 3.3	0.082
RVSP (mmHg)	37.6 ± 4.2	39.0 ± 15.5	0.626

Data are presented as *n* (%) for categorical variables and as mean ± SD for continuous variables. LA—left atrial diameter, LAV—left atrial volume, MVmaxPG—transmitral maximal pressure gradient, MVmeanPG—transmitral mean pressure gradient, MVVTI—mitral valve velocity–time integral, IVSd—interventricular septum thickness, PLWd—posterior left ventricle wall thickness at end-diastole, LVIDs—left ventricular internal dimension at end-systole, LVIDd—left ventricular internal dimension at end-diastole, EDVLV—end-diastolic volume of the left ventricle, ESVLV—end-systolic volume of left ventricle, SVLV—stroke volume of the left ventricle, EFLV—left ventricular ejection fraction, E/E′—ratio of peak velocity of early-diastolic transmitral flow to peak velocity of early-diastolic mitral annular motion as determined using pulsed-wave Doppler, AV maxPG—aortic valve peak pressure gradient, AV meanPG—aortic valve mean pressure gradient, AVVTI—aortic valvular velocity–time integral, AO—aortic root diameter, AOvs—aortic leaflet separation diameter, AscAO—diameter of ascending aorta, RAVs—right atrial volume at end-systole, TAPSE—tricuspid annular plane systolic excursion, RVSP—right ventricle systolic pressure, *—statistically significant.

Table 10. Electrocardiography (variant in *TNNT2* vs. variant not detected).

	<i>TNNT2</i>	Not Detected	<i>p</i> -Value
Sinus rhythm	5 (80.0)	8 (100.0)	0.231
Atrial flutter	0 (0.0)	0 (0.0)	-
Atrial fibrillation	2 (33.3)	0 (0.0)	0.078
Paroxysmal supraventricular tachycardia	0 (0.0)	1 (12.5)	0.369
Non-sustained ventricular tachycardia	2 (33.3)	0 (0.0)	0.078
Pacemaker	0 (0.0)	0 (0.0)	-
Heart rate (bpm)	64.0 ± 10.0	62.7 ± 5.2	0.789
Atrioventricular block I	0 (0.0)	0 (0.0)	-
Atrioventricular block II (Mobitz 1)	0 (0.0)	0 (0.0)	-
Atrioventricular block II (Mobitz 2)	0 (0.0)	0 (0.0)	-
Atrioventricular block III	0 (0.0)	0 (0.0)	-
Left bundle branch block	1 (16.7)	1 (12.5)	0.825
Right bundle branch block	2 (33.3)	0 (0.0)	0.078
Left anterior hemiblock	1 (16.7)	1 (12.5)	0.825
Right anterior hemiblock	0 (0.0)	0 (0.0)	-
PR interval (ms)	172.6 ± 17.0	170.5 ± 23.6	0.867
QRS duration (ms)	111.5 ± 30.5	96.1 ± 17.9	0.258
Sokolow index (mm)	24.2 ± 9.2	26.9 ± 13.1	0.648
Significant Q wave	2 (33.3)	2 (25.0)	0.733
ST segment abnormalities	2 (33.3)	6 (75.0)	0.119
Negative T wave	4 (66.7)	7 (87.5)	0.347

Data are presented as *n* (%) for categorical variables and as mean ± SD for continuous variables.

Tricuspid annular plane systolic excursion (TAPSE) was significantly higher in patients with a variant in *MYH7* than in patients without a detected variant (24.6 vs. 19.9 mm, *p* = 0.028) (Table 5). Calcification of mitral annulus was less common in patients with a variant in the *MYBPC3* gene than in those without a detected variant (6 vs. 50%, *p* = 0.013) (Table 7), and the same applies to ST segment abnormalities (31 vs. 75%, *p* = 0.043) (Table 8). Calcification of mitral annulus was also less common in patients with a variant in the *TNNT2* gene than in those without a detected variant (0 vs. 50%, *p* = 0.040) (Table 9), and end-systolic volume of left ventricle (ESVLV) was lower in patients with a variant in the *TNNT2* gene than in those without a detected variant (22.7 vs. 41.7 mL, *p* = 0.029) (Table 9).

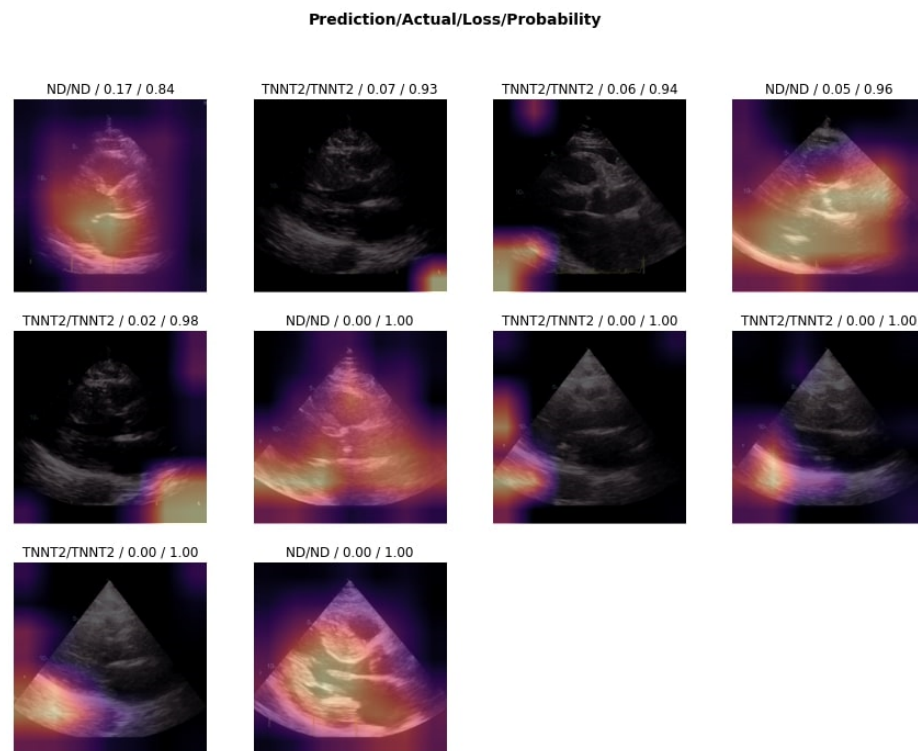


Figure 14. Discriminative areas for classification of a given image (variant in *TNNT2* vs. variant not detected), parasternal long-axis view during ventricular diastole. The deeper the highlighted color, the more relevant the region is for a particular class prediction.

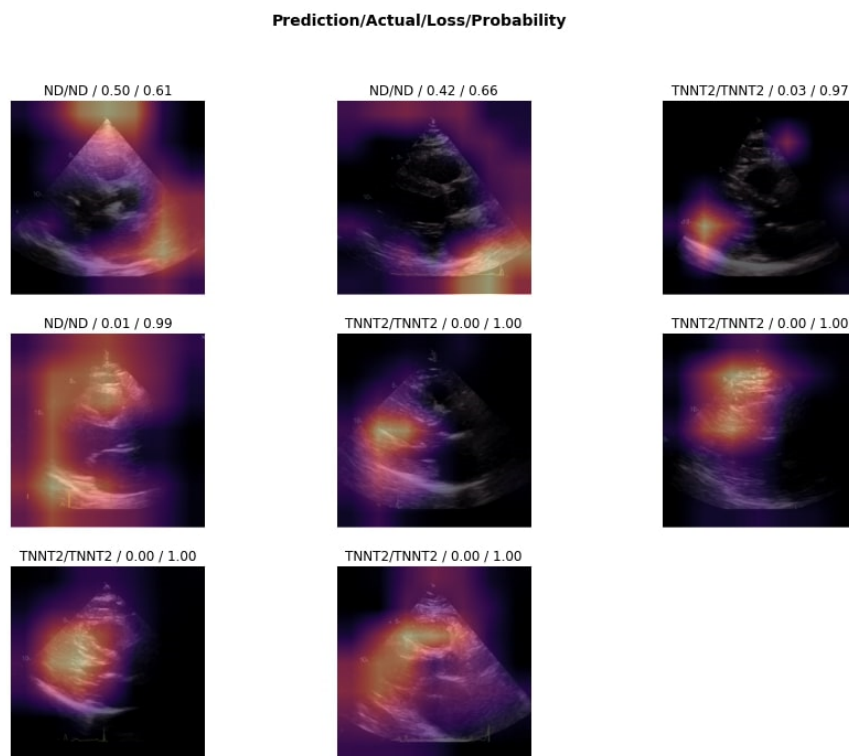


Figure 15. Discriminative areas for classification of a given image (variant in *TNNT2* vs. variant not detected), parasternal long-axis view during ventricular systole. The deeper the highlighted color, the more relevant the region is for a particular class prediction.

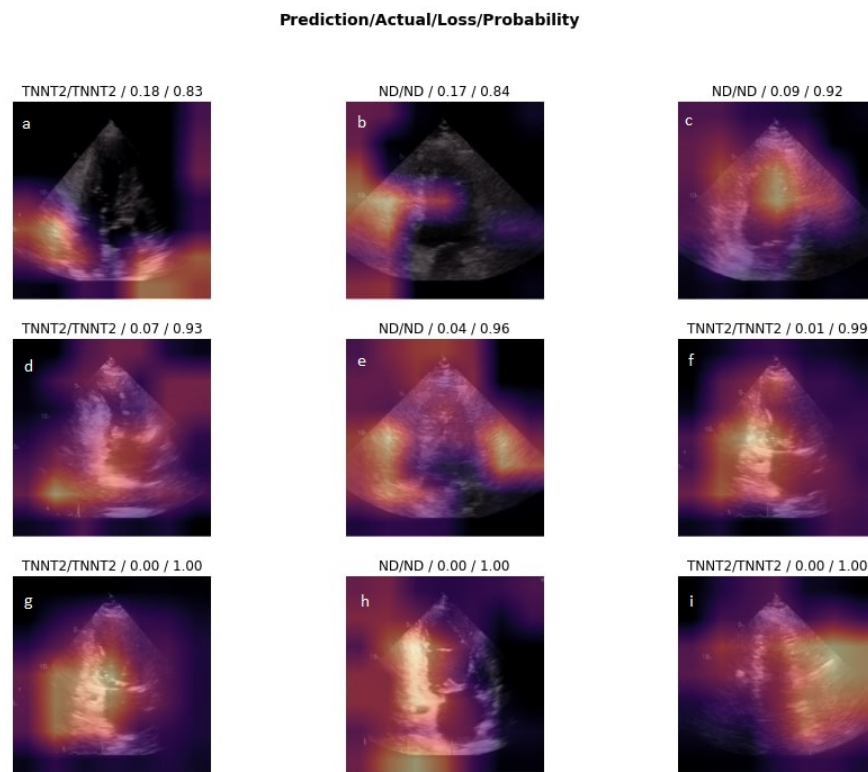


Figure 16. Discriminative areas for classification of a given image (variant in *TNNT2* vs. variant not detected), apical 2-chamber view during ventricular diastole. The deeper the highlighted color, the more relevant the region is for a particular class prediction.

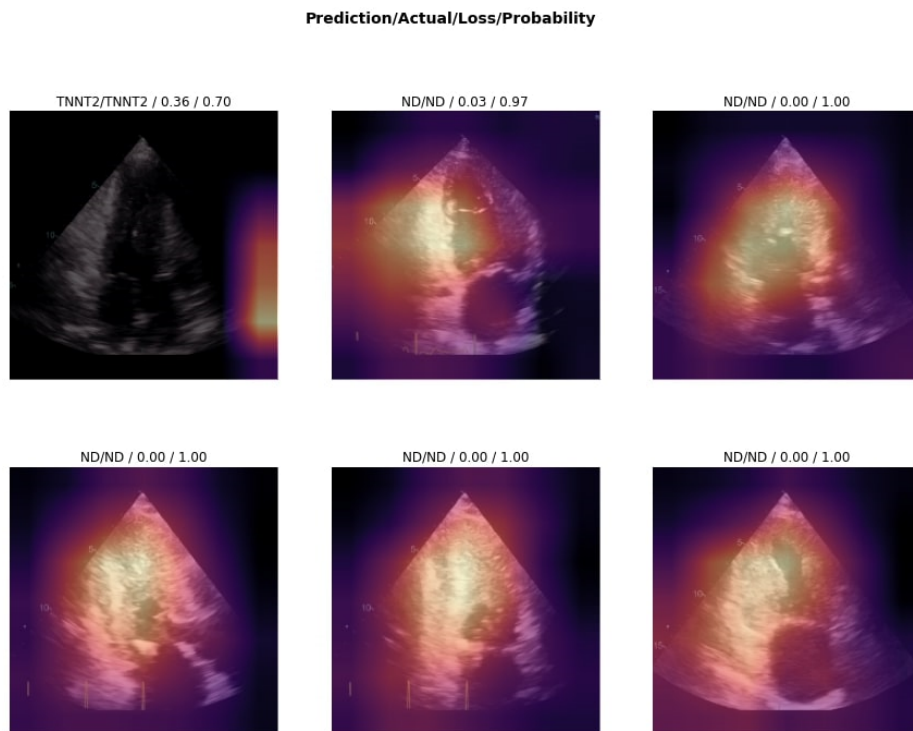


Figure 17. Discriminative areas for classification of a given image (variant in *TNNT2* vs. variant not detected), apical 2-chamber view during ventricular systole. The deeper the highlighted color, the more relevant the region is for a particular class prediction.

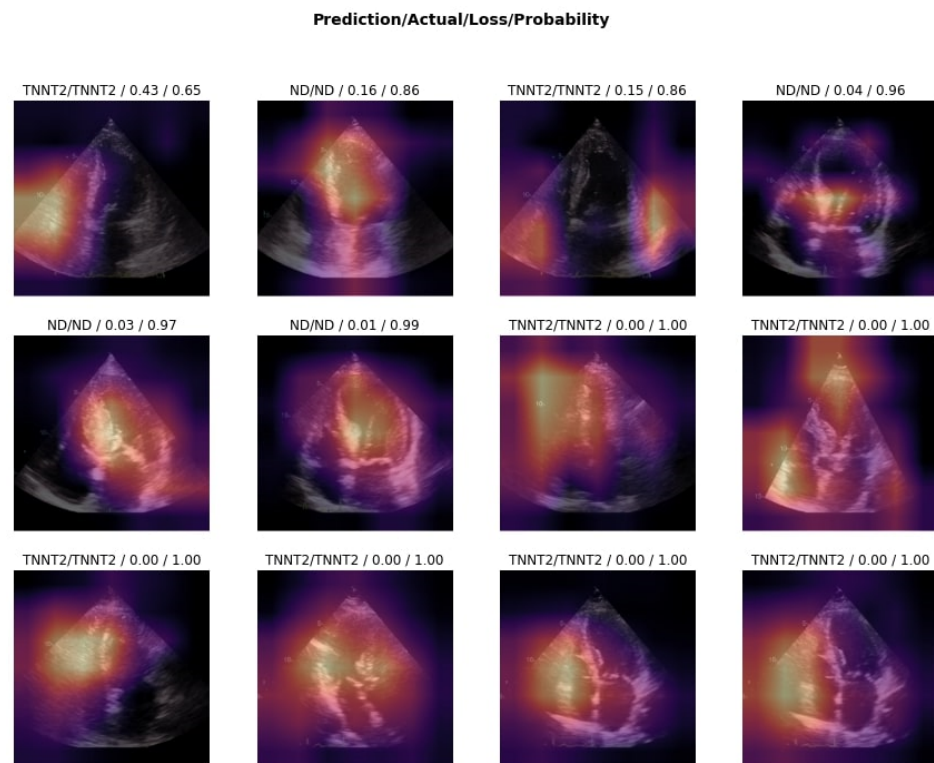


Figure 18. Discriminative areas for classification of a given image (variant in *TNNT2* vs. variant not detected), apical 4-chamber view during ventricular diastole. The deeper the highlighted color, the more relevant the region is for a particular class prediction.

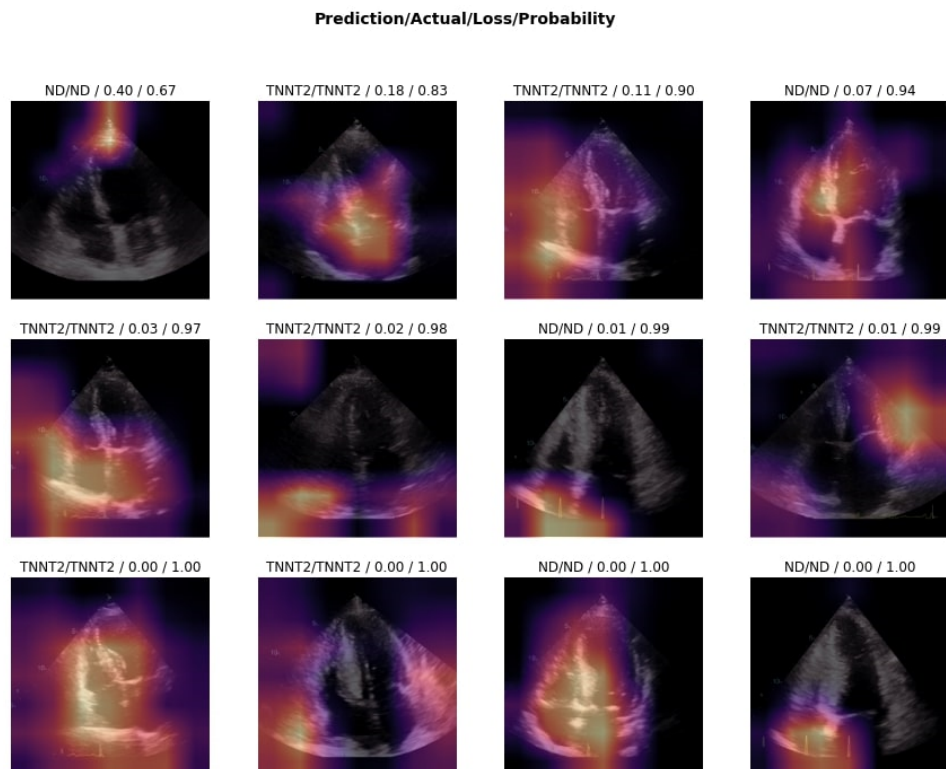


Figure 19. Discriminative areas for classification of a given image (variant in *TNNT2* vs. variant not detected), apical 4-chamber view during ventricular systole. The deeper the highlighted color, the more relevant the region is for a particular class prediction.

4. Discussion

This study detected potential cardiac regions affected by structural outcomes of variants in *MYH7*, *MYBPC3*, and *TNNT2*.

Analyzing the results regarding one of the parameters of the longitudinal systolic function of the right ventricle—TAPSE, for the variant in *MYH7* compared to HCM where variant was not detected (the right ventricular systolic function is better in *MYH7*), the results are fully consistent with the images (Figure 7, middle row) as well as with other parameters, albeit statistically nonsignificant: left ventricular ejection function (LVEF), which is higher in the *MYH7* group.

Similar observations relate to the calcification of the mitral annulus. It is less pronounced in the variant in *MYBPC3* compared to HCM where variant was not detected. The results are in complete alignment with the images (Figure 10—multiple images, and also Figure 12—only images b and p). In these cases as well, although statistically nonsignificant, LVEF is higher in the *MYBPC3* group, also is longitudinal systolic function of the right ventricle (TAPSE).

In the case of variant in *TNNT2*, the calcification of the mitral annulus is less compared to HCM where variant was not detected. The results are completely consistent with Figure 16 (images g and h). In these cases as well, although statistically nonsignificant, LVEF and TAPSE are better in the *MYBPC3* group.

It is well known that the longitudinal systolic function of the right ventricle is a predictor of outcomes in patients who have left ventricular disease (valvular disease, ischemic disease, cardiomyopathies), so it is reasonable that it is better if the left ventricular systolic function is better. In later clinical course, we can of course expect a worsening of the longitudinal systolic function of the right ventricle despite the preserved ejection fraction of the left ventricle.

4.1. *MYH7*

The septum, left ventricular outflow tract (LVOT) segment, anterior wall, apex, right ventricle, and mitral apparatus were shown to be discriminative for the classification of echocardiographic images of patients with a variant in the *MYH7* gene and those without a detected variant.

MYH7 is one of the two most common causal genes in the usual form of HCM with the involvement of the basal septum and apical HCM [15]. Li et al. described a case of HCM with a variant in *MYH7* and significantly hypertrophied systolic interventricular septum [48]. Van de Sande et al. described a case with myocardial crypts found in the anterior septum in a carrier of the variant in *MYH7* [49]. In the study by Gruner et al. on a genetically tested cohort of 61 patients with apical HCM, sarcomere protein gene variants were most often found in the *MYH7* and *MYBPC3* genes [50]. In the study by Chung et al., among 212 patients, pathogenic variants in sarcomere-associated genes were more prevalent in non-apical HCM than in apical HCM, and the variant frequency in the *MYH7* gene was 9% in the cases of apical HCM [51]. In the study by Velicki et al. involving 63 HCM *MYBPC3*- or *MYH7*-variant positive patients, calcifications of mitral annulus were found only in patients with a variant in the *MYH7* gene, and mitral leaflet abnormalities were significantly more often in patients with a variant in the *MYH7* gene [52]. Waldmüller et al. reported a link between variants in *MYH7* and a higher degree of mitral valve regurgitation in HCM [53].

4.2. *MYBPC3*

The septum, left ventricle, and left ventricle/chamber were shown to be discriminative for the classification of echocardiographic images of patients with a variant in the *MYBPC3* gene and those without a detected variant.

MYBPC3 is one of the two most common causal genes in the usual form of HCM with the involvement of the basal septum [15]. Tarkiainen et al. reported that subjects with the *MYBPC3*-Q10961X variant have increased left ventricular septal convexity irrespective of

the presence of left ventricular hypertrophy [54]. Waldmüller et al. reported a link between variants in *MYBPC3* and a particularly large thickness of the interventricular septum [53].

4.3. *TNNT2*

The septum and right ventricle were shown to be discriminative for the classification of echocardiographic images of patients with a variant in the *TNNT2* gene and those without a detected variant.

In a study by Mori et al., *TNNT2* p.Lys263Arg was shown to be associated with increased septum thickness [55].

4.4. Limitations

The number of patients and images used to train and validate the models is considerably small for an image classification task. The results presented in this study cannot be used to make any definitive overarching conclusions because the sample size used in this research is relatively small. While the initial results may provide some insights, they should be interpreted with caution and serve as a basis for future research with larger and more representative samples. The examined sample is to a certain extent homogenic. These findings need further confirmation with a larger sample and/or in clinical settings.

These models are not intended to assist in any diagnostic decision-making; nonetheless, they can be used as a potential basis for further clinical research.

Depending on the depth of coverage, the TruSight Cardio Sequencing Panel may be insufficient to allow for single-exon or larger copy-number variation detection/inference, which could prevent identifying 3–5% of potentially pathogenic/likely pathogenic events [56].

Since the aim of this study was to find structures that computer algorithms would choose to use to distinguish carriers of variants in specific causal genes (vs. variant not detected) in HCM patients, and not to develop a state-of-the-art model for finding the structures that indicate the presence of variants in these genes in the general population, the design did not include a control cohort of healthy patients. The performance shown only indicates that the performance assessed in this sample is high, and therefore, that it is reasonable to expect that discriminatory structures for this sample were found. The structures found are the main results of this research, while the performance shown is only an argument to support their discriminativeness in this sample and for this sample.

4.5. Future Perspectives

By conducting this smaller-scale study, we were able to uncover initial trends and patterns, which can guide the development of larger, more comprehensive studies in the future. This was, at the same time, the main purpose of this study: to establish a potential starting point for the future discovery of structural outcomes of variants in main causative HCM genes. Future studies can build upon this foundation and use larger sample sizes to corroborate and refine the initial observations made in this research. Future research could also explore the usage of our methods for other relevant HCM differentiations, e.g., within the same family, to find whether minor phenotypical features may discriminate carriers from non-carriers.

5. Conclusions

This study detected potential cardiac regions affected by structural outcomes of variants in the main causative HCM genes. Gene-specific discriminative echocardiogram findings were identified: for variants in the *MYH7* gene (vs. variant not detected), the most discriminative structures are the septum, LVOT segment, anterior wall, apex, right ventricle, and mitral apparatus; for variants in the *MYBPC3* gene (vs. variant not detected), these are the septum, left ventricle, and left ventricle/chamber; while for variants in the *TNNT2* gene (vs. variant not detected), the most discriminative structures are the septum and right ventricle.

Supplementary Materials: The following supporting information can be downloaded at: <https://www.mdpi.com/article/10.3390/cardiogenetics14010001/s1>, Table S1. Detected variants.

Author Contributions: Conceptualization, M.G., A.I. and L.V.; methodology, M.G. and L.V.; software, M.G. and L.V.; formal analysis, M.G.; investigation, M.G.; resources, A.I. and L.V.; data curation, M.G. and A.I.; writing—original draft preparation, M.G.; writing—review and editing, M.G., A.I. and L.V.; visualization, M.G. and A.I.; supervision, L.V.; project administration, M.G.; funding acquisition, L.V. All authors have read and agreed to the published version of the manuscript.

Funding: This research was funded by the Autonomous Province of Vojvodina—Projects of importance for the development of scientific research activities (2021–2024) under contract No. 142-451-2568/2021-01.

Institutional Review Board Statement: Not applicable.

Informed Consent Statement: Not applicable.

Data Availability Statement: Data are available upon reasonable request. The data are not publicly available due to privacy and ethical restrictions.

Conflicts of Interest: The authors declare no conflict of interest.

References

1. Geske, J.B.; Ommen, S.R.; Gersh, B.J. Hypertrophic cardiomyopathy: Clinical update. *JACC Heart Fail.* **2018**, *6*, 364–375. [[CrossRef](#)]
2. Zegkos, T.; Tziomalos, G.; Parcharidou, D.; Ntelios, D.; Papanastasiou, C.A.; Karagiannidis, E.; Gossios, T.; Rouskas, P.; Katranas, S.; Paraskevaidis, S.; et al. Validation of the new American College of Cardiology / American Heart Association Guidelines for the risk stratification of sudden cardiac death in a large Mediterranean cohort with Hypertrophic Cardiomyopathy. *Hell. J. Cardiol.* **2022**, *63*, 15–21. [[CrossRef](#)]
3. Sabater-Molina, M.; Pérez-Sánchez, I.; Hernández Del Rincón, J.P.; Gimeno, J.R. Genetics of hypertrophic cardiomyopathy: A review of current state. *Clin. Genet.* **2018**, *93*, 3–14. [[CrossRef](#)]
4. de Oliveira Antunes, M.; Scudeler, T.L. Hypertrophic cardiomyopathy. *Int. J. Cardiol. Heart Vasc.* **2020**, *27*, 100503.
5. Maron, B.J.; Desai, M.Y.; Nishimura, R.A.; Spirito, P.; Rakowski, H.; Towbin, J.A.; Dearani, J.A.; Rowin, E.J.; Maron, M.S.; Sherrid, M.V. Management of hypertrophic cardiomyopathy: JACC state-of-the-art review. *J. Am. Coll. Cardiol.* **2022**, *79*, 390–414. [[CrossRef](#)]
6. Glavaški, M.; Velicki, L. Shared molecular mechanisms of hypertrophic cardiomyopathy and its clinical presentations: Automated molecular mechanisms extraction approach. *Life* **2021**, *11*, 785. [[CrossRef](#)]
7. Bonaventura, J.; Polakova, E.; Vejtasova, V.; Veselka, J. Genetic testing in patients with hypertrophic cardiomyopathy. *Int. J. Mol. Sci.* **2021**, *22*, 10401. [[CrossRef](#)]
8. Semsarian, C.; Ingles, J.; Maron, M.S.; Maron, B.J. New perspectives on the prevalence of hypertrophic cardiomyopathy. *J. Am. Coll. Cardiol.* **2015**, *65*, 1249–1254. [[CrossRef](#)]
9. Prondzynski, M.; Mearini, G.; Carrier, L. Gene therapy strategies in the treatment of hypertrophic cardiomyopathy. *Pflugers Arch.* **2019**, *471*, 807–815. [[CrossRef](#)]
10. Wolf, C.M. Hypertrophic cardiomyopathy: Genetics and clinical perspectives. *Cardiovasc. Diagn. Ther.* **2019**, *9*, S388–S415. [[CrossRef](#)]
11. Younger, J.; Lo, A.; McCormack, L.; McGaughan, J.; Prasad, S.; Atherton, J.J. Hypertrophic cardiomyopathy: Challenging the status quo? *Heart Lung Circ.* **2020**, *29*, 556–565. [[CrossRef](#)] [[PubMed](#)]
12. Cao, Y.; Zhang, P.Y. Review of recent advances in the management of hypertrophic cardiomyopathy. *Eur. Rev. Med. Pharmacol. Sci.* **2017**, *21*, 5207–5210. [[PubMed](#)]
13. Hayashi, T. Hypertrophic cardiomyopathy: Diverse pathophysiology revealed by genetic research, toward future therapy. *Keio J. Med.* **2020**, *69*, 77–87. [[CrossRef](#)] [[PubMed](#)]
14. Weissler-Snir, A.; Allan, K.; Cunningham, K.; Connelly, K.A.; Lee, D.S.; Spears, D.A.; Rakowski, H.; Dorian, P. Hypertrophic cardiomyopathy-related sudden cardiac death in young people in Ontario. *Circulation* **2019**, *140*, 1706–1716. [[CrossRef](#)] [[PubMed](#)]
15. Marian, A.J.; Braunwald, E. Hypertrophic cardiomyopathy: Genetics, pathogenesis, clinical manifestations, diagnosis, and therapy. *Circ. Res.* **2017**, *121*, 749–770. [[CrossRef](#)] [[PubMed](#)]
16. Jordà, P.; Oudit, G.Y.; Tadros, R. Unraveling the genetic substrate and phenotypic variability of hypertrophic cardiomyopathy: A role for desmosome gene variants? *Can. J. Cardiol.* **2022**, *38*, 3–5. [[CrossRef](#)] [[PubMed](#)]
17. Pai, S.L.; Chadha, R.M.; Logvinov, I.I.; Brigham, T.J.; Watt, K.D.; Li, Z.; Palmer, W.C.; Blackshear, J.L.; Aniskevich, S. Preoperative echocardiography as a prognostic tool for liver transplant in patients with hypertrophic cardiomyopathy. *Clin. Transplant.* **2022**, *36*, e14538. [[CrossRef](#)] [[PubMed](#)]
18. Preveden, A.; Golubovic, M.; Bjelobrk, M.; Miljkovic, T.; Ilic, A.; Stojsic, S.; Glavaski, M.; Maier, L.S.; Okwose, N.; Popovic, D. Gender related differences in the clinical presentation of hypertrophic cardiomyopathy—An analysis from the SILICOFCM database. *Medicina* **2022**, *58*, 314. [[CrossRef](#)]

19. Aguiar Rosa, S.; Rocha Lopes, L.; Fiarresga, A.; Ferreira, R.C.; Mota Carmo, M. Coronary microvascular dysfunction in hypertrophic cardiomyopathy: Pathophysiology, assessment, and clinical impact. *Microcirculation* **2021**, *28*, e12656. [[CrossRef](#)]
20. Hong, Y.; Su, W.W.; Li, X. Risk factors of sudden cardiac death in hypertrophic cardiomyopathy. *Curr. Opin. Cardiol.* **2022**, *37*, 15–21. [[CrossRef](#)]
21. Zhang, M.; Sun, X.; Wu, G.; Wang, D.; Wang, L.; Zhang, C.; Zou, Y.; Wang, J.; Song, L. Effect of cis-compound variants in *MYH7* on hypertrophic cardiomyopathy with a mild phenotype. *Am. J. Cardiol.* **2022**, *167*, 104–110. [[CrossRef](#)]
22. Wu, G.; Liu, J.; Ruan, J.; Yu, S.; Wang, L.; Zhao, S.; Wang, S.; Kang, L.; Wang, J.; Song, L. Deleterious rare desmosomal variants contribute to hypertrophic cardiomyopathy and are associated with distinctive clinical features. *Can. J. Cardiol.* **2022**, *38*, 41–48. [[CrossRef](#)]
23. van der Velden, J.; Stienen, G.J.M. Cardiac disorders and pathophysiology of sarcomeric proteins. *Physiol. Rev.* **2019**, *99*, 381–426. [[CrossRef](#)]
24. Wijnker, P.J.M.; Sequeira, V.; Kuster, D.W.D.; van der Velden, J. Hypertrophic cardiomyopathy: A vicious cycle triggered by sarcomere mutations and secondary disease hits. *Antioxid. Redox. Signal.* **2019**, *31*, 318–358. [[CrossRef](#)]
25. Huang, H.; Chen, Y.; Jin, J.; Du, R.; Tang, K.; Fan, L.; Xiang, R. *CSRP3*, p.Arg122*, is responsible for hypertrophic cardiomyopathy in a Chinese family. *J. Gene Med.* **2022**, *24*, e3390. [[CrossRef](#)]
26. Teekakirikul, P.; Zhu, W.; Huang, H.C.; Fung, E. Hypertrophic cardiomyopathy: An overview of genetics and management. *Biomolecules* **2019**, *9*, 878. [[CrossRef](#)]
27. Arif, M.; Nabavizadeh, P.; Song, T.; Desai, D.; Singh, R.; Bazrafshan, S.; Bazrafshan, S.; Kumar, M.; Wang, Y.; Gilbert, R.J.; et al. Genetic, clinical, molecular, and pathogenic aspects of the South Asian-specific polymorphic *MYBPC3*^{Δ25bp} variant. *Biophys. Rev.* **2020**, *12*, 1065–1084. [[CrossRef](#)]
28. Yotti, R.; Seidman, C.E.; Seidman, J.G. Advances in the genetic basis and pathogenesis of sarcomere cardiomyopathies. *Annu. Rev. Genom. Hum. Genet.* **2019**, *20*, 129–153. [[CrossRef](#)]
29. Chou, C.; Chin, M.T. Pathogenic mechanisms of hypertrophic cardiomyopathy beyond sarcomere dysfunction. *Int. J. Mol. Sci.* **2021**, *22*, 8933. [[CrossRef](#)]
30. Mazzarotto, F.; Olivotto, I.; Boschi, B.; Girolami, F.; Poggesi, C.; Barton, P.J.R.; Walsh, R. Contemporary insights into the genetics of hypertrophic cardiomyopathy: Toward a new era in clinical testing? *J. Am. Heart Assoc.* **2020**, *9*, e015473. [[CrossRef](#)]
31. Glavaški, M.; Velicki, L. Humans and machines in biomedical knowledge curation: Hypertrophic cardiomyopathy molecular mechanisms' representation. *BioData Min.* **2021**, *14*, 45. [[CrossRef](#)] [[PubMed](#)]
32. Norrish, G.; Field, E.; Kaski, J.P. Childhood hypertrophic cardiomyopathy: A disease of the cardiac sarcomere. *Front. Pediatr.* **2021**, *9*, 708679. [[CrossRef](#)] [[PubMed](#)]
33. Ommen, S.R.; Semsarian, C. Hypertrophic cardiomyopathy: A practical approach to guideline directed management. *Lancet* **2021**, *398*, 2102–2108. [[CrossRef](#)] [[PubMed](#)]
34. Makavos, G.; Kairis, C.; Tselegkidi, M.E.; Karamitsos, T.; Rigopoulos, A.G.; Noutsias, M.; Ikonomidis, I. Hypertrophic cardiomyopathy: An updated review on diagnosis, prognosis, and treatment. *Heart Fail. Rev.* **2019**, *24*, 439–459. [[CrossRef](#)] [[PubMed](#)]
35. Popa-Fotea, N.M.; Micheu, M.M.; Bataila, V.; Scafa-Udriste, A.; Dorobantu, L.; Scarlatescu, A.I.; Zamfir, D.; Stoian, M.; Onciul, S.; Dorobantu, M. Exploring the continuum of hypertrophic cardiomyopathy—From DNA to clinical expression. *Medicina* **2019**, *55*, 299. [[CrossRef](#)] [[PubMed](#)]
36. Glavaški, M.; Preveden, A.; Jakovljević, Đ.; Filipović, N.; Velicki, L. Subtypes and mechanisms of hypertrophic cardiomyopathy proposed by machine learning algorithms. *Life* **2022**, *12*, 1566. [[CrossRef](#)] [[PubMed](#)]
37. Shamout, F.; Zhu, T.; Clifton, D.A. Machine learning for clinical outcome prediction. *IEEE Rev. Biomed. Eng.* **2021**, *14*, 116–126. [[CrossRef](#)]
38. Barragán-Montero, A.; Javaid, U.; Valdés, G.; Nguyen, D.; Desbordes, P.; Macq, B.; Willems, S.; Vandewinckele, L.; Holmström, M.; Löfman, F.; et al. Artificial intelligence and machine learning for medical imaging: A technology review. *Phys. Med.* **2021**, *83*, 242–256. [[CrossRef](#)]
39. Shi, Q.; Chen, W.; Huang, S.; Wang, Y.; Xue, Z. Deep learning for mining protein data. *Brief. Bioinform.* **2021**, *22*, 194–218. [[CrossRef](#)]
40. Quer, G.; Arnaout, R.; Henne, M.; Arnaout, R. Machine learning and the future of cardiovascular care: JACC state-of-the-art review. *J. Am. Coll. Cardiol.* **2021**, *77*, 300–313. [[CrossRef](#)]
41. Tran, K.A.; Kondrashova, O.; Bradley, A.; Williams, E.D.; Pearson, J.V.; Waddell, N. Deep learning in cancer diagnosis, prognosis and treatment selection. *Genome Med.* **2021**, *13*, 152. [[CrossRef](#)] [[PubMed](#)]
42. Hallou, A.; Yevick, H.G.; Dumitrascu, B.; Uhlmann, V. Deep learning for bioimage analysis in developmental biology. *Development* **2021**, *148*, dev199616. [[CrossRef](#)] [[PubMed](#)]
43. Wang, H.; Pujos-Guillot, E.; Comte, B.; de Miranda, J.L.; Spiwok, V.; Chorbev, I.; Castiglione, F.; Tieri, P.; Watterson, S.; McAllister, R.; et al. Deep learning in systems medicine. *Brief. Bioinform.* **2021**, *22*, 1543–1559. [[CrossRef](#)] [[PubMed](#)]
44. Chan, H.P.; Samala, R.K.; Hadjiiski, L.M.; Zhou, C. Deep learning in medical image analysis. *Adv. Exp. Med. Biol.* **2020**, *1213*, 3–21. [[PubMed](#)]

45. Tafelmeier, M.; Baessler, A.; Wagner, S.; Unsoeld, B.; Preveden, A.; Barlocco, F.; Tomberli, A.; Popovic, D.; Brennan, P.; MacGowan, G.A.; et al. Design of the SILICOFM study: Effect of sacubitril/valsartan vs lifestyle intervention on functional capacity in patients with hypertrophic cardiomyopathy. *Clin. Cardiol.* **2020**, *43*, 430–440. [[CrossRef](#)] [[PubMed](#)]
46. Glavaški, M.; Velicki, L. More slices, less truth: Effects of different test-set design strategies for magnetic resonance image classification. *Croat. Med. J.* **2022**, *63*, 370–378. [[CrossRef](#)] [[PubMed](#)]
47. Selvaraju, R.R.; Cogswell, M.; Das, A.; Vedantam, R.; Parikh, D.; Batra, D. Grad-CAM: Visual explanations from deep networks via gradient-based localization. *Int. J. Comput. Vis.* **2020**, *128*, 336–359. [[CrossRef](#)]
48. Li, X.; Tang, J.; Li, J.; Lin, S.; Wang, T.; Zhou, K.; Li, Y.; Hua, Y. Genetic clues on implantable cardioverter-defibrillator placement in young-age hypertrophic cardiomyopathy: A case report of novel *MYH7* mutation and literature review. *Front. Cardiovasc. Med.* **2021**, *8*, 810291. [[CrossRef](#)]
49. van de Sande, D.A.; Hoogsteen, J.; Theunissen, L.J. An unusual presentation of a myocardial crypt in hypertrophic cardiomyopathy. *Case Rep. Cardiol.* **2014**, *2014*, 737052. [[CrossRef](#)]
50. Gruner, C.; Care, M.; Siminovitch, K.; Moravsky, G.; Wigle, E.D.; Woo, A.; Rakowski, H. Sarcomere protein gene mutations in patients with apical hypertrophic cardiomyopathy. *Circ. Cardiovasc. Genet.* **2011**, *4*, 288–295. [[CrossRef](#)]
51. Chung, H.; Kim, Y.; Cho, S.M.; Lee, H.J.; Park, C.H.; Kim, J.Y.; Lee, S.H.; Min, P.K.; Yoon, Y.W.; Lee, B.K.; et al. Differential contributions of sarcomere and mitochondria-related multigene variants to the endophenotype of hypertrophic cardiomyopathy. *Mitochondrion* **2020**, *53*, 48–56. [[CrossRef](#)] [[PubMed](#)]
52. Velicki, L.; Jakovljevic, D.G.; Preveden, A.; Golubovic, M.; Bjelobrck, M.; Ilic, A.; Stojsic, S.; Barlocco, F.; Tafelmeier, M.; Okwose, N.; et al. Genetic determinants of clinical phenotype in hypertrophic cardiomyopathy. *BMC Cardiovasc. Disord.* **2020**, *20*, 516. [[CrossRef](#)] [[PubMed](#)]
53. Waldmüller, S.; Erdmann, J.; Binner, P.; Gelbrich, G.; Pankuweit, S.; Geier, C.; Timmermann, B.; Haremza, J.; Perrot, A.; Scheer, S.; et al. Novel correlations between the genotype and the phenotype of hypertrophic and dilated cardiomyopathy: Results from the German Competence Network Heart Failure. *Eur. J. Heart Fail.* **2011**, *13*, 1185–1192. [[CrossRef](#)] [[PubMed](#)]
54. Tarkiainen, M.; Sipola, P.; Jalanko, M.; Heliö, T.; Jääskeläinen, P.; Kivelä, K.; Laine, M.; Lauerma, K.; Kuusisto, J. CMR derived left ventricular septal convexity in carriers of the hypertrophic cardiomyopathy-causing *MYBPC3*-Q1061X mutation. *Sci. Rep.* **2019**, *9*, 5960. [[CrossRef](#)]
55. Mori, A.A.; Castro, L.R.; Bortolin, R.H.; Bastos, G.M.; Oliveira, V.F.; Ferreira, G.M.; Hirata, T.D.C.; Fajardo, C.M.; Sampaio, M.F.; Moreira, D.A.R.; et al. Association of variants in *MYH7*, *MYBPC3* and *TNNT2* with sudden cardiac death-related risk factors in Brazilian patients with hypertrophic cardiomyopathy. *Forensic Sci. Int. Genet.* **2021**, *52*, 102478. [[CrossRef](#)]
56. Truty, R.; Paul, J.; Kennemer, M.; Lincoln, S.E.; Olivares, E.; Nussbaum, R.L.; Aradhya, S. Prevalence and properties of intragenic copy-number variation in Mendelian disease genes. *Genet. Med.* **2019**, *21*, 114–123. [[CrossRef](#)]

Disclaimer/Publisher’s Note: The statements, opinions and data contained in all publications are solely those of the individual author(s) and contributor(s) and not of MDPI and/or the editor(s). MDPI and/or the editor(s) disclaim responsibility for any injury to people or property resulting from any ideas, methods, instructions or products referred to in the content.